

# NAVAL POSTGRADUATE SCHOOL Monterey, California

2

AD-A245 952



DTIC  
ELECTE  
FEB 13 1992  
S B D

## THESIS

A CONTINUING STUDY OF ALTITUDE DETERMINATION  
DEFICIENCIES OF THE SERVICE AIRCRAFT  
INSTRUMENTATION PACKAGE (SAIP)

by

Robert J. Russell

SEPTEMBER 1991

Thesis Advisor:

O. Biblarz

Approved for public release: Distribution is unlimited

92-03467



REPORT DOCUMENTATION PAGE				Form Approved OMB No 0704-0188	
1a. REPORT SECURITY CLASSIFICATION <b>Unclassified</b>			1b. RESTRICTIVE MARKINGS		
2a. SECURITY CLASSIFICATION AUTHORITY		3. DISTRIBUTION/AVAILABILITY OF REPORT <b>Approved for public release: Distribution is unlimited</b>			
2b. DECLASSIFICATION/DOWNGRADING SCHEDULE					
4. PERFORMING ORGANIZATION REPORT NUMBER(S)			5. MONITORING ORGANIZATION REPORT NUMBER(S)		
6a. NAME OF PERFORMING ORGANIZATION <b>Naval Postgraduate School</b>		6b. OFFICE SYMBOL <i>(If applicable)</i> <b>AA</b>	7a. NAME OF MONITORING ORGANIZATION <b>Naval Postgraduate School</b>		
6c. ADDRESS <i>(City, State and ZIP Code)</i> <b>Monterey, CA 93943-5000</b>			7b. ADDRESS <i>(City, State, and ZIP Code)</i> <b>Monterey, CA 93943-5000</b>		
8a. NAME OF FUNDING/SPONSORING ORGANIZATION		8b. OFFICE SYMBOL <i>(If applicable)</i>	9. PROCUREMENT INSTRUMENT IDENTIFICATION NUMBER		
8c. ADDRESS <i>(City, State, and ZIP Code)</i>			10. SOURCE OF FUNDING NUMBER		
			PROGRAM ELEMENT NO.	PROJECT NO.	TASK NO.
11. TITLE <i>(Include Security Classification)</i> <b>A CONTINUING STUDY OF ALTITUDE DETERMINATION DEFICIENCIES OF THE SERVICE AIRCRAFT INSTRUMENTATION PACKAGE (SAIP)</b>					
12. PERSONAL AUTHORS <b>ROBERT J. RUSSELL</b>					
13a. TYPE OF REPORT <b>Master's Thesis</b>		13b. TIME COVERED FROM _____ TO _____	14. DATE OF REPORT <i>(Year, Month, Day)</i> <b>SEPTEMBER 1991</b>		15. PAGE COUNT <b>80</b>
16. SUPPLEMENTARY NOTATION <b>The views expressed are those of the author and do not reflect the official policy or position of the Department of Defense or the U.S. Government</b>					
17. COSATI CODES			18. SUBJECT TERMS <i>(Continue on reverse if necessary and identify by block numbers)</i> <b>altitude determination errors, static pressure measurement, probe design</b>		
FIELD	GROUP	SUB-GROUP			
19. ABSTRACT <i>(Continue on reverse if necessary and identify by block numbers)</i> <p>After correcting test equipment used in a previous study of the SAIP for an ambiguous grounding requirement, research was continued on aerodynamic factors affecting SAIP altitude measurement. Existing equations for incompressible flow over a cylinder and a sphere were used to model the static-pressure probe located on the front of the SAIP pod and an algorithm was derived for the computation of the pressure coefficient, <math>C_p</math>. Our low-speed wind tunnel data show an overpressure at the static pressure ports when the angle of attack (<math>\phi</math>) is less than <math>14^\circ</math>. The five-inch diameter body of the SAIP, located aft of the static pressure probe, is responsible for creating a stagnation-like region at the front of the SAIP probe which envelops the static-port location. Calculation of the altitude error (<math>\Delta Z</math>) using the model for <math>C_p</math>, corrected for compressibility, is within <math>\pm 15\%</math> of the error observed in flight at Mach 0.60. Improvements in the compressibility correction as well as analyses using an aero-panel method are suggested before sufficiently reliable fixes to the SAIP can be proposed.</p>					
20. DISTRIBUTION/AVAILABILITY OF ABSTRACT <input checked="" type="checkbox"/> UNCLASSIFIED/UNLIMITED <input type="checkbox"/> SAME AS RPT <input type="checkbox"/> DTIC USERS			21. ABSTRACT SECURITY CLASSIFICATION <b>unclassified</b>		
22a. NAME OF RESPONSIBLE INDIVIDUAL <b>O. Biblarz</b>			22b. TELEPHONE <i>(Include Area Code)</i> <b>(408) 646-3096</b>		22c. OFFICE SYMBOL <b>AA/Bi</b>

Approved for public release: Distribution is unlimited

A Continuing Study of Altitude Determination Deficiencies  
of the Service Aircraft Instrumentation Package (SAIP)

by

Robert J. Russell  
Lieutenant, United States Naval Reserve  
B.S., Oregon State University, 1980

Submitted in partial fulfillment of the  
requirements for the degree of

MASTER OF SCIENCE  
IN AERONAUTICAL ENGINEERING

from the

NAVAL POSTGRADUATE SCHOOL

SEPTEMBER 1991

Author:

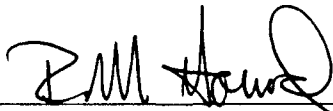


Robert J. Russell

Approved by:



O. Biblarz, Thesis Advisor



R.M. Howard, Second Reader



D.J. Collins, Chairman  
Department of Aeronautical Engineering



## TABLE OF CONTENTS

I.	INTRODUCTION .....	1
	A. BACKGROUND .....	1
	1. System Description .....	1
	2. System Performance .....	1
	B. THESIS PURPOSE .....	4
II.	THEORY .....	5
	A. ELEMENTARY FLOW ANALYSIS .....	5
	B. COMPRESSIBILITY EFFECT .....	9
	C. FLOW SEPARATION STUDY .....	12
	D. ALTITUDE ERROR DETERMINATION .....	15
III.	WIND TUNNEL PROCEDURES AND DATA .....	17
	A. WIND TUNNEL APPARATUS .....	17
	1. Wind Tunnel .....	17
	2. Service Aircraft Instrumentation Package (SAIP) .....	20
	a. General .....	20
	b. Nose Cone Assembly .....	20
	c. Airflow Sensor Assembly .....	22
	d. Air-Data Unit (ADU) .....	22
	e. SAIP Calibration .....	25
	3. Nose Cone Assembly (NCA) Mounting Assembly .....	25
	4. Instrumentation .....	27
	B. WIND TUNNEL DATA .....	29
	1. Results Before Ground-Fix .....	29
	2. Data After Ground-Fix .....	30
	3. Elevation Defect ( $\Delta Z$ ) .....	35
	4. Flow Visualization .....	37

IV.	FLIGHT TEST .....	40
	A. TACTS POD .....	40
	1. Description .....	40
	2. TACTS Pod Flight Test .....	42
	B. SAIP POD .....	47
	1. Flight Test Description .....	47
	2. Test Results .....	48
V.	CONCLUSIONS AND RECOMMENDATIONS .....	53
	A. CONCLUSIONS .....	53
	1. Analysis .....	53
	2. Wind Tunnel Tests .....	54
	3. Flight Testing .....	55
	B. RECOMMENDATIONS .....	55
APPENDIX A:	NCA WIND TUNNEL TEST DATA ( $\Delta$ VOLTS UNCORRECTED) .....	57
APPENDIX B:	TACTS POD FLIGHT TEST DATA .....	59
APPENDIX C:	TEST PLAN .....	60
APPENDIX D:	SAIP FLIGHT TEST DATA (27 SEPT 89) .....	66
	LIST OF REFERENCES .....	67
	INITIAL DISTRIBUTION LIST .....	68

## LIST OF FIGURES

Figure 1.	Service Aircraft Instrumentation Package (SAIP); Configuration -003 [Ref. 1:p. 10]. . . . .	2
Figure 2.	Configuration For Flow Around a Circular Cylinder. . . . .	5
Figure 3.	Theoretical Incompressible $C_p$ . . . . .	8
Figure 4.	Pressure Distribution Over a Symmetrical Wing. . . . .	9
Figure 5.	Plot of Equation (8) With Göthert Compressibility Correction. . . . .	11
Figure 6.	Vortex Generation Regimes [Ref. 8]. . . . .	13
Figure 7.	Naval Postgraduate School Wind Tunnel [Ref. 11]. . . . .	18
Figure 8.	Nose Cone Assembly (NCA) [Ref. 1]. . . . .	21
Figure 9.	Airflow Sensor Assembly (ASA) [Ref. 1]. . . . .	23
Figure 10.	Calibration of SAIP (Volts/psia). . . . .	26
Figure 11.	NCA Mounting Assembly (side view). . . . .	27
Figure 12.	Power Supply Module. . . . .	28
Figure 13.	Pressure Difference of SAIP and Atmosphere. . . . .	31
Figure 14.	SAIP #0040; Wind Tunnel Data vs. Theory. . . . .	33
Figure 15.	SAIP #0040; Wind Tunnel Data vs Theory. . . . .	34
Figure 16.	Converted Theoretical $C_p$ to $\Delta Z$ (feet). . . . .	36
Figure 17a.	Photograph of SAIP and Tufts Where $\phi = 0^\circ$ . . . . .	38
Figure 17b.	Photograph of SAIP and Tufts Where $\phi = 15^\circ$ . . . . .	38
Figure 18.	Tactical Aircrew Combat Training System (TACTS) Pod. . . . .	41
Figure 19.	A-6 Aircraft and Wing Stations. . . . .	43
Figure 20.	Static Pressure Altitude Versus Indicated Mach Number. . . . .	45
Figure 21.	TACTS Pod Altitude Determination (10,000 ft). . . . .	46

Figure 22.	Altitude Error Determination ( $\Delta Z$ ). Comparison of Equation (20) to SAIP Flight Test Data. . . . .	50
Figure 23.	Altitude Error Determination. Comparison of Equation (20) to SAIP Flight Test Data. . . . .	52

## NOMENCLATURE

a	Local speed of sound
AOA	Angle-of-attack
ADU	Air Data Unit
ASA	Airflow Sensor Assembly
$C_{po}$	Incompressible coefficient of pressure
$C_p$	Coefficient of pressure
$\delta$	Ellipsoid thickness ratio
$\gamma$	Specific heat of gases
DPU/DIU	Data Processing Unit/Data Interface Unit
DVM	Digital voltmeter
EATS	Extended Area Tracking System
g	Gravitational constant
$\theta$	Angle of rotation about SAIP longitudinal axis
IMN	Indicated Mach number
KIAS	Knots indicated air speed
$\lambda$	Lapse rate
M	Local Mach number
$M_\infty$	Free-stream Mach number
NATOPS	Naval Air Training and Operating Procedures Standardization
NCA	Nose Cone Assembly
NPS	Naval Postgraduate School
NSWC	Naval Strike Warfare Center
P	Local pressure
$P_\infty$	Free-stream pressure
P3	Total pressure

P(A1), P(A2)	Differential angle-of-attack pressures
P(B1), P(B2)	Differential angle-of-sideslip pressures
$P_s$	Static pressure
PMTC	Pacific Missile Test Center
$\rho$	Gas density
R	Gas constant
SAIP	Service Aircraft Instrumentation Package
T	Local temperature
$T_\infty$	Free-stream temperature
TACTS	Tactical Aircrew Combat Training System
$U_m$	Measured wind tunnel velocity
V	Local velocity
$V_\infty$	Free-stream velocity
$\phi$	Angle of rotation about SAIP vertical axis
Z	Altitude

## **ACKNOWLEDGEMENTS**

The assistance and support of a number of people have been instrumental in the completion of this project. I wish to thank Prof. Oscar Biblarz for his unending guidance and patience. Although numerous people at PMTC contributed to this research, I wish to specifically thank Messrs. John Loos, Dave Muskat, Guy Cooper, Brian Frankhouser and Randy Ray. In addition, flight test data provided by LT Brian Reeves, NSWC, was greatly appreciated. Finally, I am deeply indebted to my family and fiancée, Shannon, for their moral support.

# I. INTRODUCTION

## A. BACKGROUND

### 1. System Description

The Service Aircraft Instrumentation Package (SAIP) is an airborne pod configured to mount on aircraft equipped with the LAU-7/A (series) launcher or equivalent. Operating within the Extended Area Tracking System (EATS), Pacific Missile Test Center (PMTTC), Point Mugu, CA, the SAIP was designed to provide independent three dimensional tracking information on aircraft functioning within the test range. The SAIP consists of a five-inch diameter stainless steel tube which houses the majority of the electronic subassemblies, and a fiberglass nose cone with an integral air data subsystem and antenna subsystem (Figure 1). Avionics within the SAIP enable the tracking station to obtain range, altitude, airspeed, attitude, and weapon-system data from the aircraft. The SAIP requires only primary AC and DC power from the host aircraft and communicates with the tracking system through its antenna system which receives and radiates signals at 141 MHz. The main purpose of the air flow sensor is to provide barometric pressures for altitude determination. [Ref. 1: p. 90]

### 2. System Performance

Performance specifications state that "altitude error in 50 percent of the track updates shall be less than the larger of 100 ft or three percent of the participant altitude [Ref. 1: p. 144]". However, initial flight test in May 1989 showed altitude errors in excess

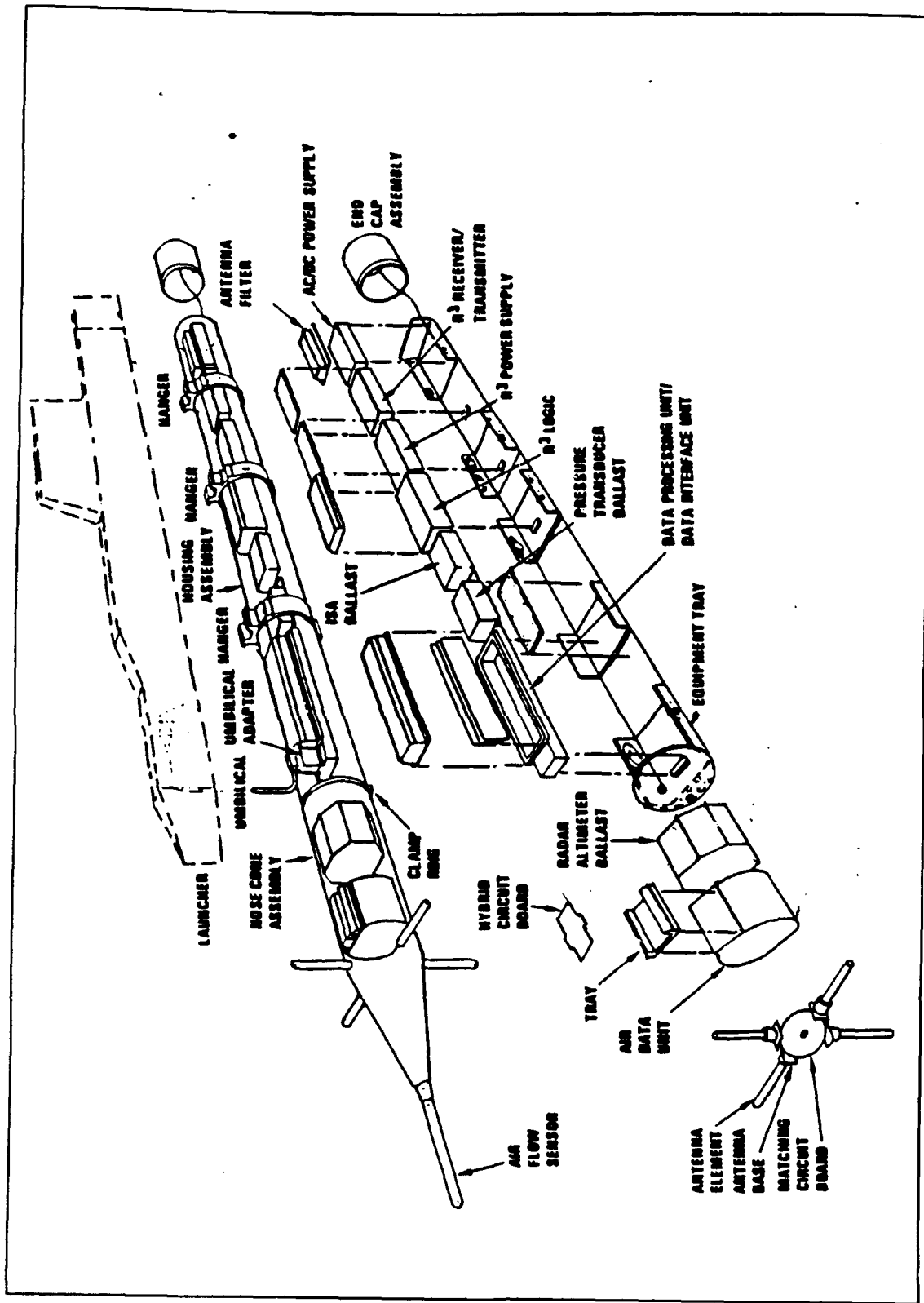


Figure 1. Service Aircraft Instrumentation Package (SAIP); Configuration -003 [Ref. 1:p. 10].

of specifications. Preflight checks showed correct altitudes, but at an altitude of 4,000 ft and at flight speeds ranging from 375-500 kts, altitude errors of about 420 ft below known altitude were reported [Ref. 2]. Additional flight tests on 7 Sept 1989 flown at 4,000 and 10,000 feet showed that higher airspeeds and elevations substantially aggravated errors in the reported SAIP altitudes. Specifically, errors on the order of 500-600 ft were experienced at an altitude of 4,000 ft, and errors ranging from 900-1000 ft were observed at an altitude of 10,000 ft [Ref. 3:pp. 4-5].

Original work at NPS in the study of this altitude problem found a possible error associated with the Air Data Unit (ADU) in the form of electrical cross-talk [Ref. 3:p. 91]. It was postulated that this cross-talk accounted for erroneous voltage outputs from the transducers which were subsequently converted to inaccurate static pressure measurements. However, subsequent examination of the SAIP external power requirement specifications [Ref. 1:p. 129] revealed an ambiguous power specification by the manufacturer which had been misinterpreted. This resulted in experimental errors as the required grounding requirements were not being met.

Correction of the grounding requirements yields no cross-talk or erroneous voltages and has redirected our efforts to a study of aerodynamic effects as the source of static pressure measurement errors. Such investigation has revealed that there is an inherent error in the A-6 aircraft barometric altimeter when using only static pressure to compute altitude [Ref. 4:p. 11-11]. Furthermore, all Naval Air Training and Operating Procedures Standardization Program (NATOPS) manuals have graphs which allow aircrew to correct for altitude error for various flight conditions. Flight tests flown by an A-6

aircraft from the Naval Strike Warfare Center (NSWC) on 22 May 1991, in partial support of this thesis, validated the error corrections published in the A-6 NATOPS manual.

## **B. THESIS PURPOSE**

1. To quantify the static pressure measurement errors of the SAIP in our possession (model number S/N 0040).
2. To study and quantify sources of error in what appears to be an inherent problem in measuring static pressure correctly using pitot static tubes.
3. To propose corrections to the SAIP which would allow it to determine altitudes within published specification limits and allow its integration to the EATS system.
4. To recommend the consideration of new methods to more accurately measure static pressure.



$$C_p = 1 - 4 \sin^2 \theta \quad (1)$$

If the flow direction is oriented as in Figure 2, at an angle-theta ( $\theta$ ) on the cylinder surface and an angle-phi ( $\phi$ ) with respect to the cylinder axis, the following equation is obtained:

$$V^2 = V_\infty^2 [ 4 \sin^2 \phi \sin^2 \theta + \cos^2 \phi ] \quad (2)$$

Substitution of (2) into the incompressible form of the pressure coefficient:

$$C_p = 1 - \left( \frac{V}{V_\infty} \right)^2 \quad (3)$$

yields:

$$C_p = 1 - 4 \sin^2 \phi \sin^2 \theta + \cos^2 \phi \quad (4)$$

Integration of theta from 0 to  $2\pi$  is required because static flow measurements average out the  $\theta$ -pressure distribution. Assuming inviscid flow, we get the following result:

$$C_p = 1 - 2 \sin^2 \phi - \cos^2 \phi \quad (5)$$

The  $C_p$  computed via this theoretical method should correspond to that measured in the NPS wind tunnel if the flow remains attached as the angle- $\phi$  is varied. Examination of Equation (5) shows that when  $\phi=90^\circ$ , the theoretical value of  $C_p$ , averaged from 0 to  $2\pi$  around a two-dimensional cylinder, equals -1 and when  $\phi=0^\circ$ ,  $C_p=0$  if the ends of the cylinder are neglected.

The assumption that the end effects of the SAIP can be neglected and the entire SAIP modeled as an infinite two-dimensional circular cylinder is unrealistic. The most

obvious correction is to model the tip of the probe as a hemisphere. Reference 5 shows that the pressure distribution on the surface of a sphere is given by:

$$C_p = 1 - \frac{9}{4} \sin^2 \theta \quad (6)$$

If the SAIP could be accurately modeled as a circular cylinder with a spherical tip, it would be possible to derive an algorithm for the computation of  $C_p$ . However, an examination of Figure 1 together with NPS wind tunnel tests of the SAIP have revealed that the constants associated with the trigonometric functions in Equation (5) cannot be accurately ascertained with the simplified reasoning given above. They must be found by fitting the equation to data acquired in wind tunnel tests (Equation (7)).

$$C_p = 1 - C1 \sin^2 \phi - C2 \cos^2 \phi \quad (7)$$

Substitution for the cosine-squared term in Equation (7) and a simple algebraic manipulation gives the following:

$$C_p = (1 - C2) + (C2 - C1) \sin^2 \phi \quad (8)$$

Equation (8) indicates that the value of  $C_p$  should satisfy a sine squared curve fit when the proper values of  $C1$  and  $C2$  are chosen. Wind tunnel results, presented in the following chapter, have shown the value of  $C1$  to be a value somewhat larger than 2.0 and  $C2$  a value less than 1.0. Figure 3 is a plot of  $C_p$  computed using values of  $C1=2.5$  and  $C2=0.90$  for angles of  $\phi$  ranging from  $-20^\circ$  to  $+20^\circ$ . Notice that for angles less than  $\pm 14^\circ$ , the pressures are greater than the ambient pressure and the inferred altitude using this static pressure would be below the actual altitude.

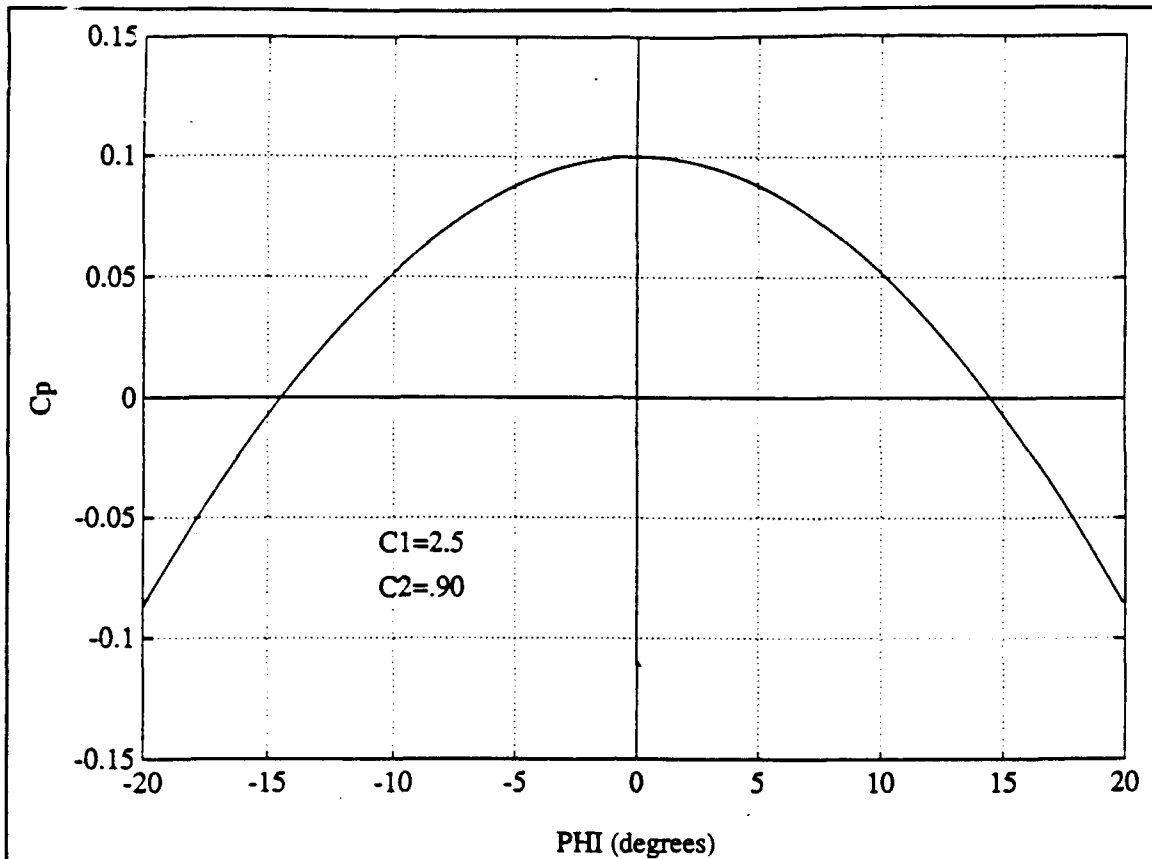


**Figure 3. Theoretical Incompressible  $C_p$ .**

It should be noted that when evaluating values measured and calculated for  $C_p$  that the five-inch diameter body of the SAIP will have an effect on the measurements read at the static ports located only six inches in front of the main five-inch diameter body. (Mr. Floyd Hagan of Rosemount, Inc., Burnville, MN, confirmed that static pressure is measured accurately by the Airflow Sensor Assembly (ASA), but that no tests were performed to study the changes which might occur when the body of the SAIP was attached to the ASA.) It is presumed that the region of  $C_p > 0$  develops at the forward tip of the probe when the angle- $\phi$  is small because of the forward stagnation region (see

Figure 4). As  $\phi$  increases, and the main body of the SAIP begins to move out of alignment with the flow impacting the pitot static probe, the flow will be more accurately modeled as a cylinder capped by a hemisphere.

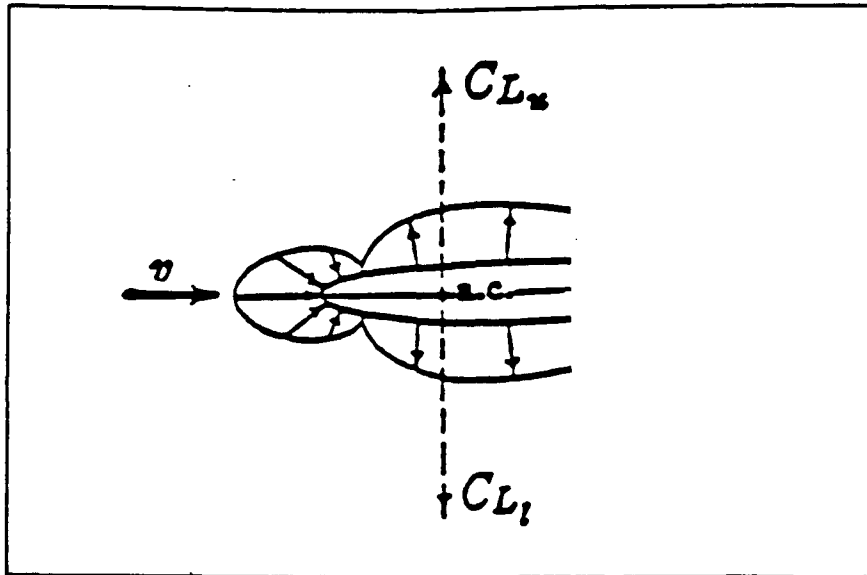


Figure 4. Pressure Distribution Over a Symmetrical Wing.

## B. COMPRESSIBILITY EFFECT

The theoretical  $C_p$  described by Equation (8) for different angles of  $\phi$  will only be accurate if the flow remains incompressible and attached throughout the flight regime. NPS wind tunnel data can be viewed as incompressible since the Mach numbers are small (less than 0.3 Mach). However, flight tests are in a compressible regime and wind tunnel data must be corrected for compressibility at high Mach numbers. This requirement necessitated the search for an accurate subsonic compressibility correction. The well-known Prandtl-Glauert correction, appropriate for two-dimensional flow, is grossly

inadequate for modeling flow over the SAIP. In a three-dimensional flow field, the result of a three-dimensional relief effect" allows the stream to deviate and must be accounted for. Thus a 3-dimensional body produces a lesser disturbance in the uniform, parallel flow, and a smaller peak pressure coefficient will result [Ref. 6]. Assuming that the SAIP pitot static probe behaves as a slender body of revolution, the Göthert Correction for a thin ellipsoid of revolution may be used [Ref. 6] to correct  $C_p$  for compressibility up to Mach numbers approaching the transonic region (Equation 9).

$$\frac{(-C_p)_{\max}}{(-C_{p_0})_{\max}} = 1 + \frac{\ell n \sqrt{1 - M_\infty^2}}{1 - \ell n 2 + \ell n \delta} \quad (9)$$

where:  $\delta$  = thickness ratio ( $t/l = 0.2$ )  
 $M_\infty$  = freestream Mach number  
 $C_{p_0}$  = pressure coefficient for incompressible flow  
 $C_p$  = pressure coefficient for compressible flow

At Mach numbers below 0.7 and angles of  $\phi$  limited to  $\pm 15^\circ$ , compressibility effects can be accurately incorporated into our model for  $C_p$  (Figure 5). The freestream Mach number ( $M_\infty$ ) amplifies the value for  $C_p$  (now  $C_{p_0}$ ) computed using Equation (8). For angle less than  $\pm 14^\circ$  the value for  $C_p$  becomes more positive, and for angles greater than  $\pm 14^\circ$   $C_p$  becomes more negative. Therefore, the effect of  $M_\infty$  on altitude-error measurements will be two-fold because the AOA (and thus  $\phi$ ) will decrease with increasing airspeed and the compressibility correction will increase  $C_p$  for any given  $\phi$ .

Studies have shown [Ref. 6] that the lower critical Mach number for a sphere is 0.57. It is conceivable that as  $\phi$  is increased from  $0^\circ$  the flow over the SAIP probe will change the critical Mach number. Therefore, we propose to limit conclusions drawn from

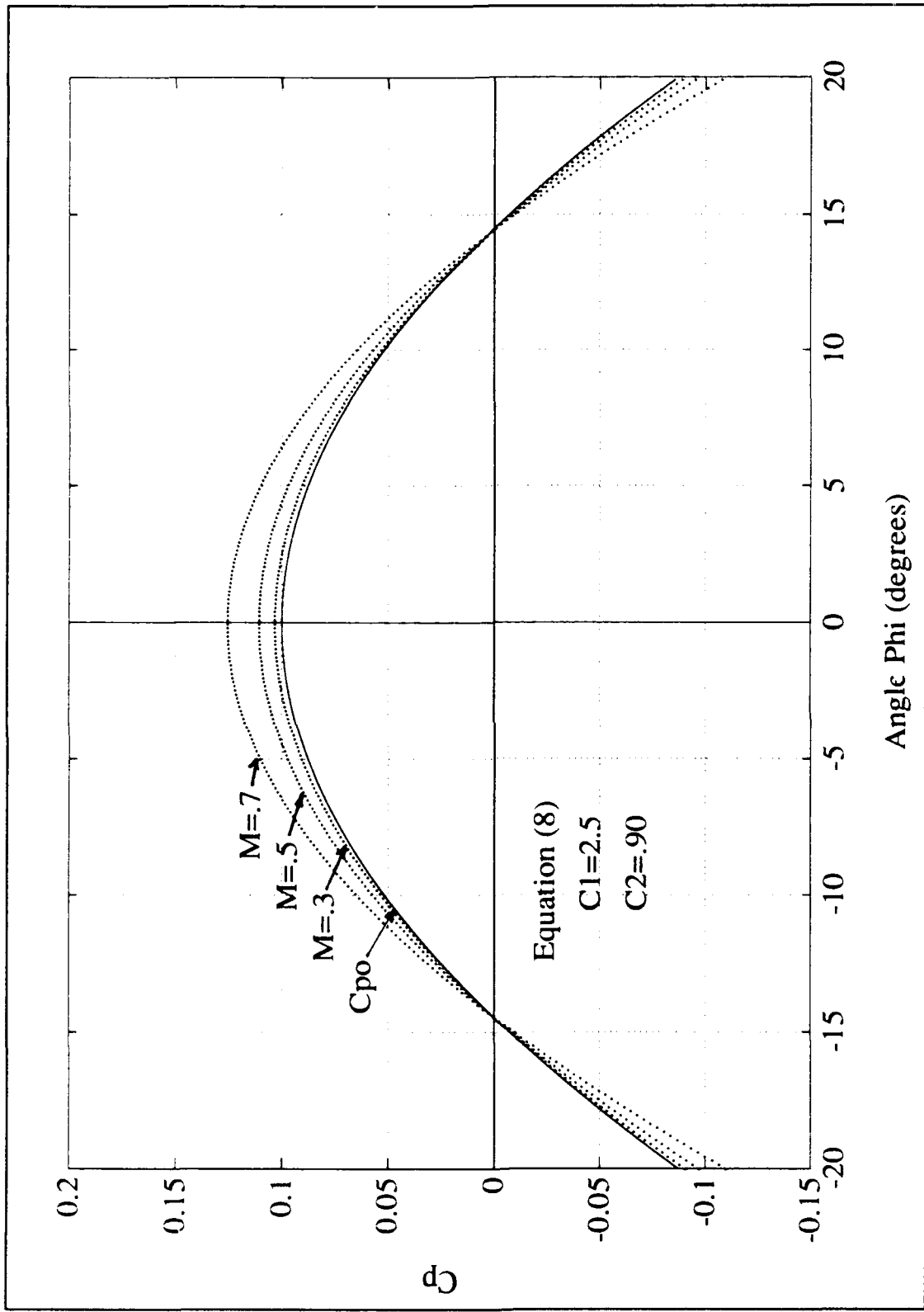


Figure 5. Plot of Equation (8) With Göthert Compressibility Correction.

theoretical calculations and flight test data to values of  $C_p$  and altitude deviations which occur at speeds below 0.7 Mach. In summary, the NPS wind tunnel allows a study of the SAIP in airflows consistent with the incompressible range of Mach numbers. The model of  $C_p$  given by Equation (8) will be corrected for compressibility, and the constants C1 and C2 determined to give the best curve fit to experimental data. These results will then allow for the prediction of  $\Delta Z$  defects as a function of  $\phi$  and  $M_\infty$ .

### C. FLOW SEPARATION STUDY

The question of flow separation must be addressed to ascertain the validity of the integration of  $\theta$  which was used to derive Equation (8). Only when the flow remains attached throughout the flight regime, will the integration of  $\theta$  from 0 to  $2\pi$  accurately represent the experimental results.

Many investigations of the aerodynamic characteristics of missiles and aircraft at high AOA have been made and reported. A "vortex system" has been found to exist in the leeward flow field of these bodies. Observations have determined that the pattern of this vortex system depends on AOA, nose geometry and roll angle, crossflow Mach number and Reynolds number, lifting surfaces, freestream turbulence, surface roughness and vibration [Ref. 7:pp. 3-4].

A slender cylinder with a pointed forebody experiences four distinct flow patterns as the AOA is varied from  $0^\circ$  to  $90^\circ$  (Figure 6). Regime III has been determined to occur at an AOA beyond  $30^\circ$  where mostly asymmetric shedding of vortices occurs [Ref. 8:pp.

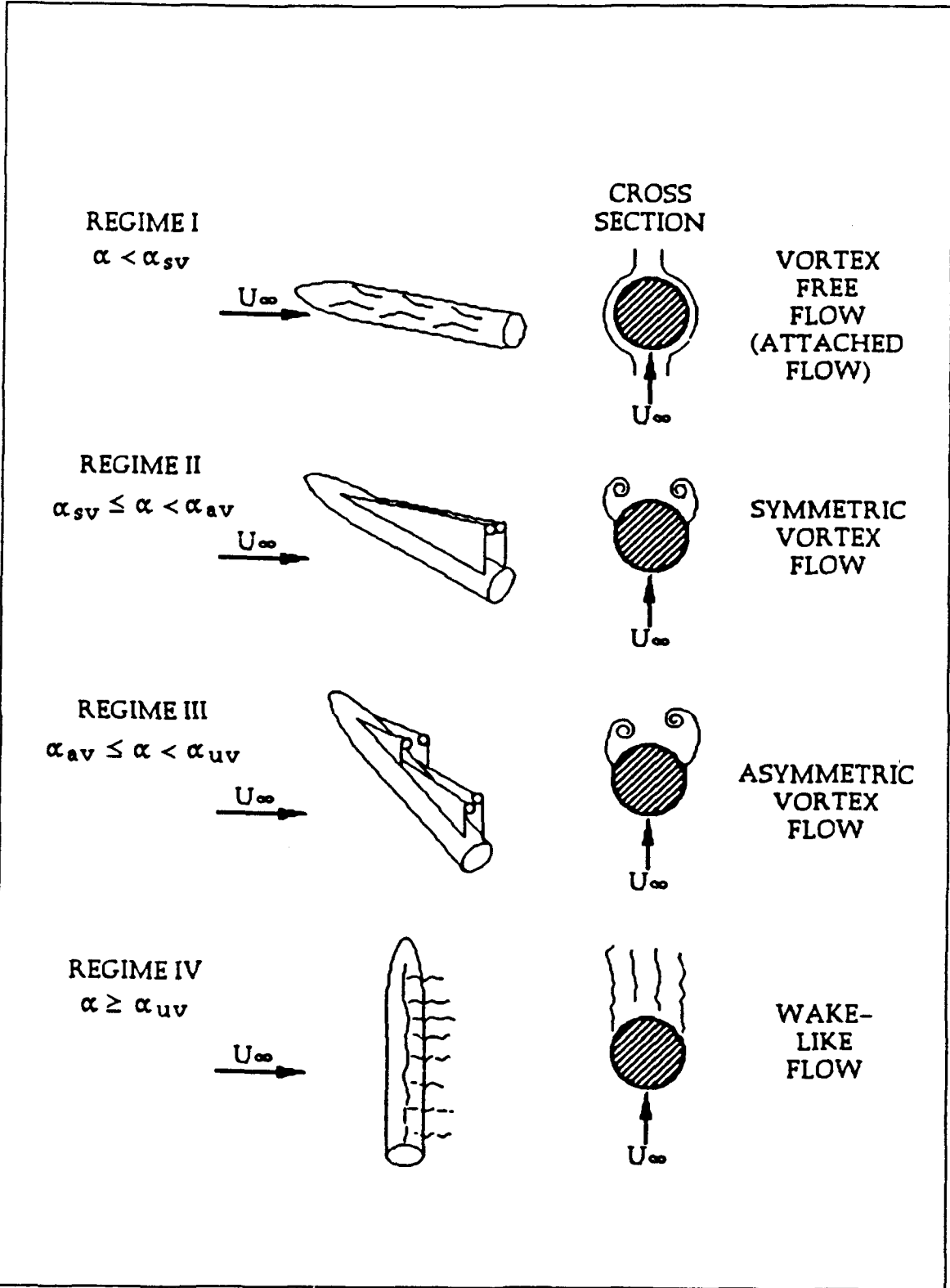


Figure 6. Vortex Generation Regimes [Ref. 8].

246-247]. The A-6 aircraft's inability to fly beyond 15° AOA suggests that we concentrate our study on regimes I and II where no set angles of demarcation exist.

Regime I is of particular interest. If it can be shown that the flow remains attached throughout the flight regime, integration of  $\theta$  over the entire periphery would be reasonable. The aircraft used for flight test, the Grumman A-6E, is not expected to exceed 25 "units" AOA, as stall will occur [Ref. 4:p. 5-28]. The AOA in degrees can be determined by converting "units", as read from the AOA gauge in the cockpit, using an algorithm determined in flight tests [Ref. 9] to be:

$$AOA ( degrees ) = 0.97523 ( units ) - 9.5989 \quad (10)$$

for the 0° flap condition.

This implies that if a probe is aligned with the aircraft longitudinal axis, the maximum AOA experienced should be 14.8°. A more probable scenario would be that the aircrew would not exceed the A-6 stall warning condition which occurs at 21 "units" and is characterized by wing rock and a gradual loss of lateral control effectiveness. This 21 "units" equates to 10.9° AOA. Now, if  $\pm 3^\circ$  is added to account for random misalignment of the SAIP and vibration of the wing, a maximum of 14° or even 15° could be expected to occur in flight. Because no definitive data are available on the angle where flow detachment will occur for the SAIP, flow visualization studies were performed (see section III.B.4).

#### D. ALTITUDE ERROR DETERMINATION

Values of delta Z ( $\Delta Z$ ) which correlate to changes in  $C_p$  may be computed in the following manner. Derivation of an algorithm for  $\Delta Z$  begins with the hydrostatic equation [Ref. 10].

$$\frac{dP}{p} = -g \frac{dZ}{RT} \quad (11)$$

Temperature of the troposphere (altitudes to 10-15 km) is approximated by:

$$\begin{aligned} T &= T_0 - \lambda Z \\ \lambda &= \text{lapse rate} = + 6.5^\circ \text{ C/km} \end{aligned} \quad (12)$$

Substitution of (12) into Equation (11) and integration yields.

$$\frac{P}{P_0} = \left( 1 - \frac{\lambda Z}{T_0} \right)^{g/\lambda R} \quad (13)$$

Substitution of (13) into (11) assuming small changes (i.e.,  $dp \cong \Delta p$ ) gives (see [Ref. 3:p. 23]):

$$\Delta P = \frac{-gP_0 \left( 1 - \frac{\lambda Z}{T_0} \right)^{g/\lambda R}}{T_0 R \left( 1 - \frac{\lambda Z}{T_0} \right)} \cdot \Delta Z \quad (14)$$

Further manipulation and substitution of the value of  $\lambda$  into Equation (14), followed by a binomial approximation, because of the small coefficient involved, gives

$$\Delta p \equiv \left[ \frac{-gP_o}{RT_o} \right] \left[ 1 - 4.25 \frac{\lambda Z}{T_o} \right] \Delta Z \quad (15)$$

Knowing that  $C_p = \frac{\Delta p}{q_\infty}$ , dividing both sides of Equation (15) by  $q_\infty$ :

$$\frac{\Delta p}{q_\infty} \equiv \frac{-1}{q_\infty} \left[ \frac{gP_o}{RT_o} \right] \left[ 1 - 4.26 \frac{\lambda Z}{T_o} \right] \Delta Z \quad (16)$$

$$C_p \equiv - \left[ \frac{g\rho_o}{.5\rho_\infty v_\infty^2} \right] \left[ 1 - 4.26 \frac{\lambda Z}{T_o} \right] \Delta Z \quad (17)$$

$$\Delta Z \equiv \frac{-C_p}{\left( 1 - 4.26 \frac{\lambda Z}{T_o} \right)} \cdot \frac{v_\infty^2}{2g} \cdot \frac{\rho_o}{\rho_\infty} \quad (18)$$

Sample calculations revealed:

$$\left( 1 - 4.26 \frac{\lambda Z}{T_o} \right) \left( \frac{\rho_o}{\rho_\infty} \right) \approx 1 \quad (19)$$

for any value of Z and the corresponding density ratio. Simplification of Equation (18) gives:

$$\Delta Z \equiv - \frac{C_p v_\infty^2}{2g} \quad (20)$$

Therefore, inasmuch as results from wind tunnel experiments can be modeled by the theoretical  $C_p$ , the values of  $C_p$  can be extended to flight conditions and be used to calculate expected  $\Delta Z$  errors due to both  $\phi$  and  $M_\infty$ .

### III. WIND TUNNEL PROCEDURES AND DATA

#### A. WIND TUNNEL APPARATUS

##### 1. Wind Tunnel

The SAIP Nose Cone Assembly (NCA) which was to serve as the test article for the various engineering analyses performed to identify the source of SAIP altitude error was provided by the PMTC Range Development Department (Code 3143). Evaluation of NCA S/N 0040, P/N 2111940-001 was performed in the Naval Postgraduate School low-speed, horizontal-flow, wind tunnel illustrated in Figure 7. This single return tunnel is powered by a 100-horsepower electric motor coupled to a three-blade variable-pitch fan via a four-speed transmission. The tunnel is 64 feet long and ranges from 21.5 to 25.5 feet wide. To straighten the flow through the tunnel, a set of stator blades have been located aft of the fan blades. Additionally, turning vanes have been installed at all four corners of the tunnel, and two fine wire mesh screens have been positioned downstream of the settling chamber to reduce turbulence. [Ref. 11]

The dimensions of the wind tunnel's test section are 45 inches by 32 inches. A reflection plane installed above the base of the test section reduces the available height in this section to 28 inches. The tunnel contraction ratio, as measured by the area of the settling chamber area divided by the test section area, is approximately 10:1. Corner fillets which are located within the test section to provide covers over four florescent lights reduce the actual section cross-sectional area from 10 ft<sup>2</sup> to 8.75 ft<sup>2</sup>. Similar fillets are

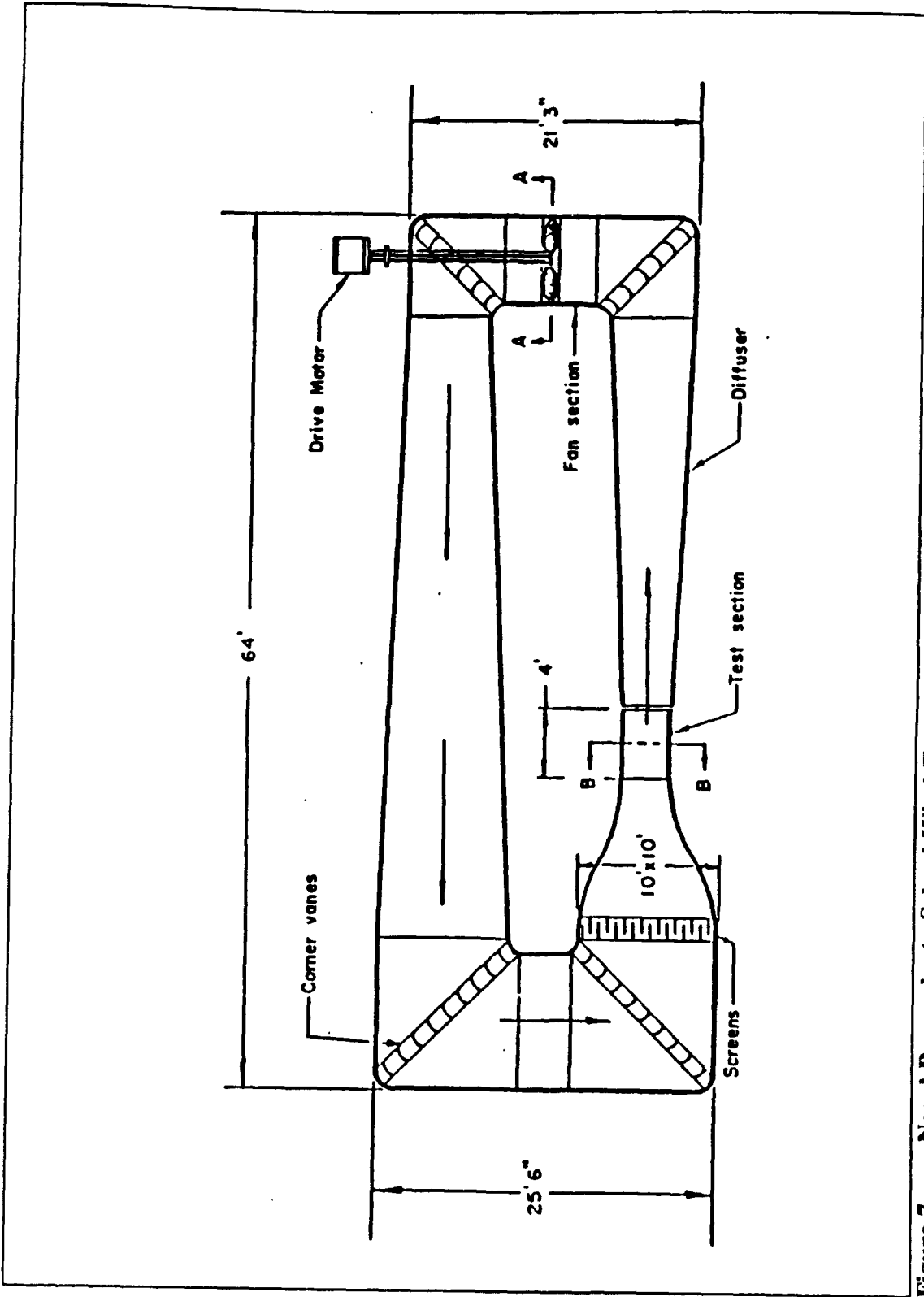


Figure 7. Naval Postgraduate School Wind Tunnel [Ref. 11].

installed at wall intersections throughout the tunnel to assist in the reduction of boundary layer effects. Prevention of the reduction in freestream pressure due to boundary layer growth within the test section is facilitated by a slight divergence of the walls in this area of the tunnel [Ref. 11].

A turntable mounted flush with the reflection plane permits operator-controlled changes in the test article pitch angle or angle of attack via a remotely controlled electric motor installed beneath the tunnel. The test section has been designed to operate at nearly atmospheric pressure, and to sustain this constant pressure, breather slots are installed around the circumference of the tunnel to replenish air lost through leakage. The tunnel was designed to generate and maintain flow velocities of up to 290 ft/sec [Ref. 11].

A dial thermometer extending into the settling chamber of the tunnel is used to measure internal tunnel temperature. Four pressure taps located upstream of the test section in the four adjoining walls are used to measure test-section reference static pressure. Additional pressure taps are located in the settling chamber section. The difference between the test section and the settling chamber pressures is used to determine dynamic pressure. This is accomplished by manifolding the separate tap pressures at the two tunnel locations into two separate lines and then connecting these outputs to a water filled manometer. The reference change in pressure measured by this manometer is displayed in centimeters of water. Equation (21) is used to calculate the actual wind tunnel velocity using the measured value of  $\Delta P$  [Ref. 11].

$$V_{\infty} = \left[ \frac{(2)(2.0475)(P)}{0.93(\rho)} \right]^{0.5} \quad (21)$$

where  $V_{\infty}$  = measured velocity (ft/sec)  
 2.0475 = conversion factor from cm H<sub>2</sub>O to lb/ft  
 P = manometer reading (cm H<sub>2</sub>O)  
 0.93 = Empirical Discharge Coefficient (correction for viscosity)  
 $\rho$  = air density (slugs/ft<sup>3</sup>)

## 2. Service Aircraft Instrumentation Package (SAIP)

### a. General

The SAIP pod used in the wind tunnel tests was a second-generation unit which incorporates hardware changes which attempt to alleviate the altitude measurement inaccuracies resulting from the first-generation pods' erroneous pressure measurements. Specifically, the second-generation unit tested was equipped with 12 static ports, each displaced by 30°, oriented about the circumference of the pod's Airflow Sensor Assembly (ASA), as opposed to the single port which existed in the first-generation unit.

### b. Nose Cone Assembly

The component of the SAIP pod used in the tests, the Nose Cone Assembly (NCA) depicted in Figure 8, performs two functions required by the SAIP. The first purpose it serves is to support the antenna subsystem which includes the matching and hybrid boards and the antenna elements. The second function of the NCA, and the one of principal concern in this study, is to support the ASA. In the particular configuration which was tested, SAIP Configuration 003, the NCA houses, in addition to the antenna subsystem and ASA, the Air-Data Unit (ADU), the radar altimeter ballast and

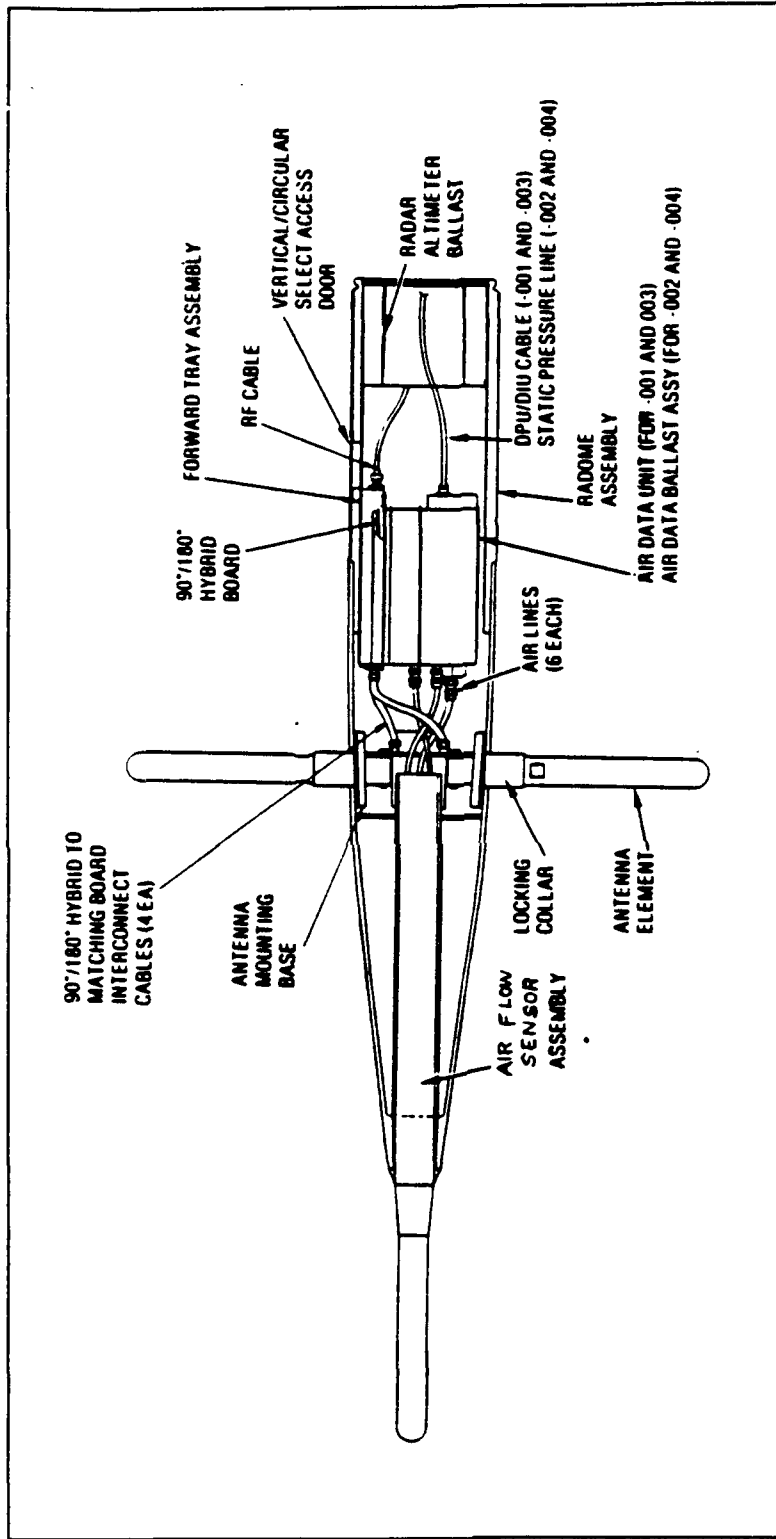


Figure 8. Nose Cone Assembly (NCA) [Ref. 1].

the antenna filter [Ref. 1:pp. 132-135]. For the purposes of the NPS wind tunnel tests, the antenna subsystem was not installed.

*c. Airflow Sensor Assembly*

The ASA consists of an airflow sensor, air lines and connectors, as illustrated in Figure 9. The function of the assembly is to provide to the ADU through six pressure lines the static pressure (one line), dynamic pressure (one line), differential angle-of-attack pressure (two lines), and differential angle-of-sideslip pressure (two lines). The airflow sensor, which is depicted in Figure 9, incorporates in a hemispherical arrangement a stagnation pressure port at its forward tip and four ports to measure differential angle-of-attack and differential angle-of-sideslip pressure, each located at 90°-offset angles. Additionally, 12 static ports which are used in the measurement of barometric altitude are situated around the pod's circumference 3.5 inches aft of the forward tip.

*d. Air-Data Unit (ADU)*

The function of the ADU is to assimilate the six pressure parameters output from the ASA and provide the analog outputs required to compute altitude, indicated airspeed, true speed, Mach number, angle-of-attack and angle-of-sideslip. On fully operational SAIP's, these analog outputs are subsequently supplied to the Data Processing Unit/Data Interface Unit (DPU/DIU) for digitizing and formatting for downlink communications [Ref. 1:p. 134]. For the purposes of this study, the ADU was not integrated with the DPU/DIU; instead, the outputs of the ADU were coupled directly to

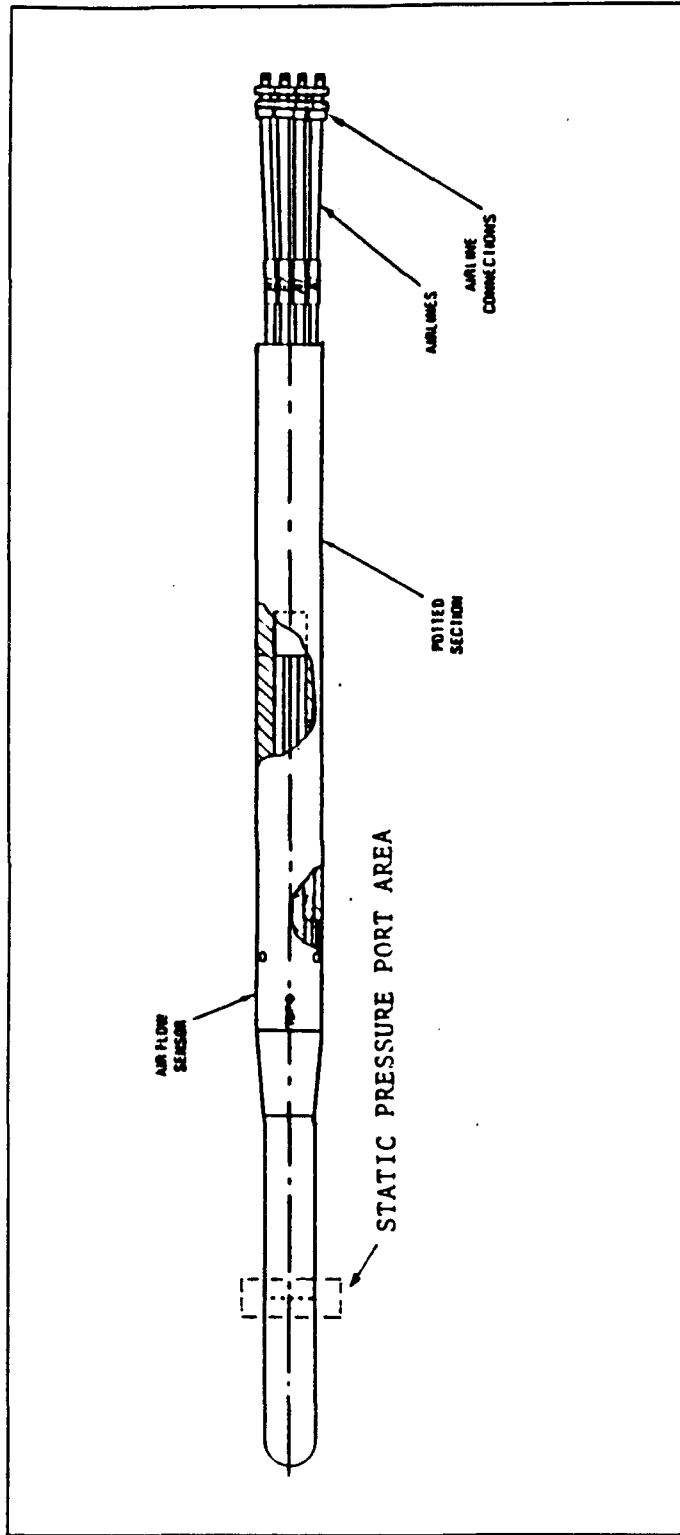


Figure 9. Airflow Sensor Assembly (ASA) [Ref. 1].

instrumentation designed to record the various output voltages from the unit, as described in Section III.A.4 below.

The ADU consists of four capacitive pressure transducers which are housed in a single assembly, as well as the associated electronic circuitry used for conditioning of the output signals from the transducers prior to their digitizing and formatting by the DPU/DIU [Ref. 1:p. 17]. Static pressure is measured by an absolute-type transducer which measures this pressure relative to a vacuum. A single static pressure line extends from the ASA into the static pressure coupler on the input side of the ADU. The remaining three transducers residing in the ADU, used to determine total, angle-of-attack and angle-of-sideslip pressures, are differential capacitive transducers. Pressure lines extend from each of the P3 (total pressure), A1, A2, B1 and B2 pressure ports on the nose of the airflow sensor and are coupled directly into the ADU in a manner similar to the static pressure line.

Once inside the ADU, the sets of angle-of-attack and angle-of-sideslip pressure lines proceed into ports situated on opposite sides of their respective differential pressure transducers. The single P3 line is directed into one side of the total pressure transducer and the other end of this transducer is coupled to the input side of the static pressure transducer (together with the static pressure input) via a one-inch long section of plastic tubing. The outputs of the four transducers are integrated with various electronic circuitry which is housed in the aft end of the ADU and which serves to condition the signals prior to digitizing and formatting for subsequent downlinking by the DPU/DIU.

***e. SAIP Calibration***

The changes in local atmospheric pressure on the static pressure transducer voltage output were recorded over a two week period. A plot of voltage vs pressure (Figure 10) was linear and provided the conversion factor used in converting wind tunnel  $\Delta$ Volts to  $\Delta$ P. It was determined from this preliminary testing that the SAIP NCA which was delivered to NPS for wind tunnel testing was calibrated in accordance with the SAIP functional specification provided with the test article [Ref. 1:p. 98].

**3. Nose Cone Assembly (NCA) Mounting Assembly**

To facilitate secure mounting of the NCA in the wind tunnel's test section and to permit orientation of the probe in a variety of flow directions, the rigid mounting assembly illustrated in Figure 11 was designed and fabricated. The mechanism was secured to the rotatable disk situated at the base of the tunnel's test section, and was extended vertically into the flow field such that the probe was held in position in the center of the flow. Rotation of the NCA about the vertical axis, representing a variation in the angle- $\phi$ , was controlled by an electric motor which permitted operator-controlled positioning of the angle of attack. Constraints imposed by the width of the wind tunnel test section restricted the rotation of the NCA about the vertical axis to  $\pm 37.5^\circ$ . Additionally, the two clamps built into the top of the V-shaped mounting saddle held the NCA securely at the top of the vertical aluminum strut and permitted the unit to be rotated  $\pm 180^\circ$  about its longitudinal axis to simulate variation in the flow angle- $\theta$ . The capability to both vertically and longitudinally rotate the NCA facilitated the simulation

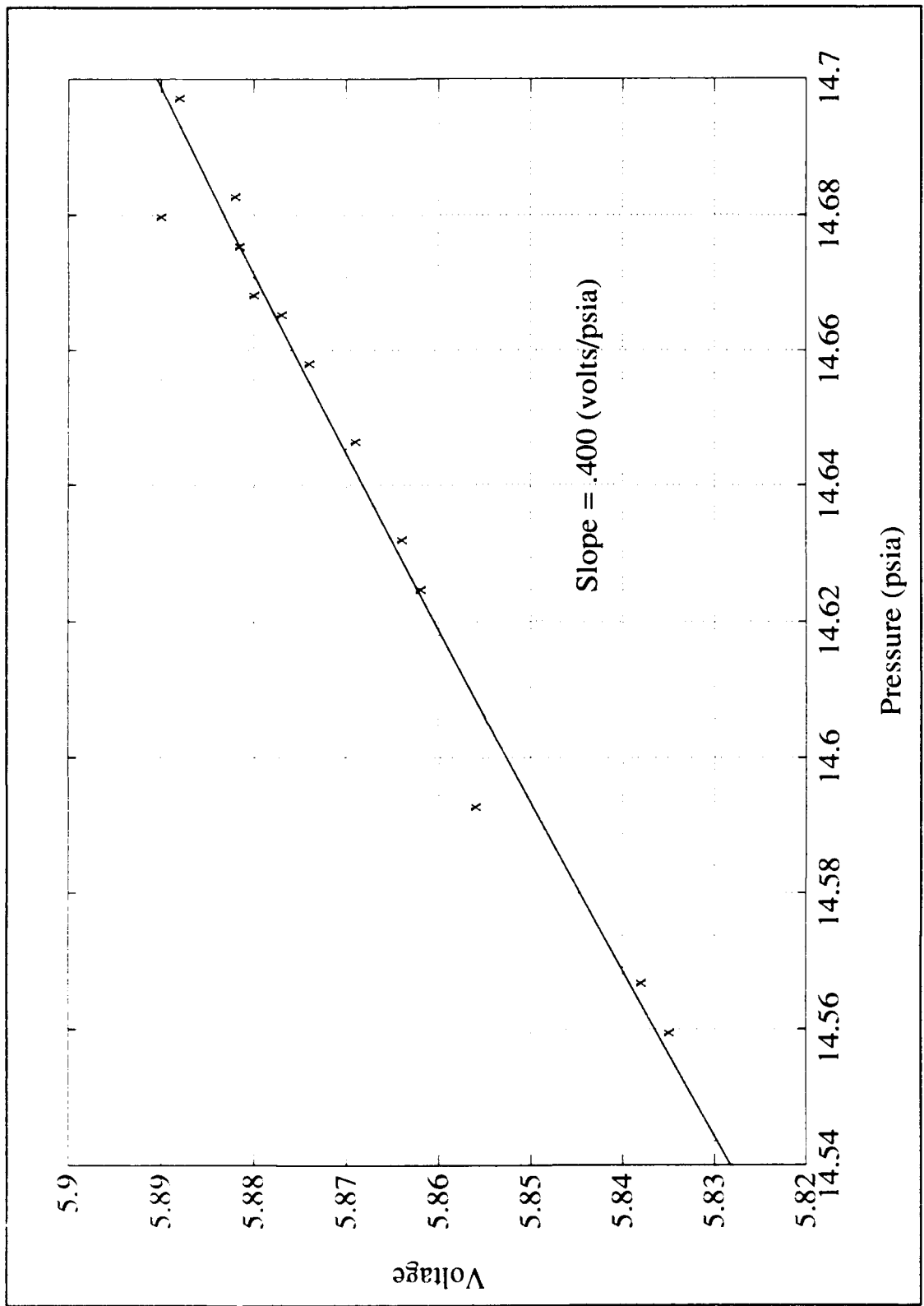
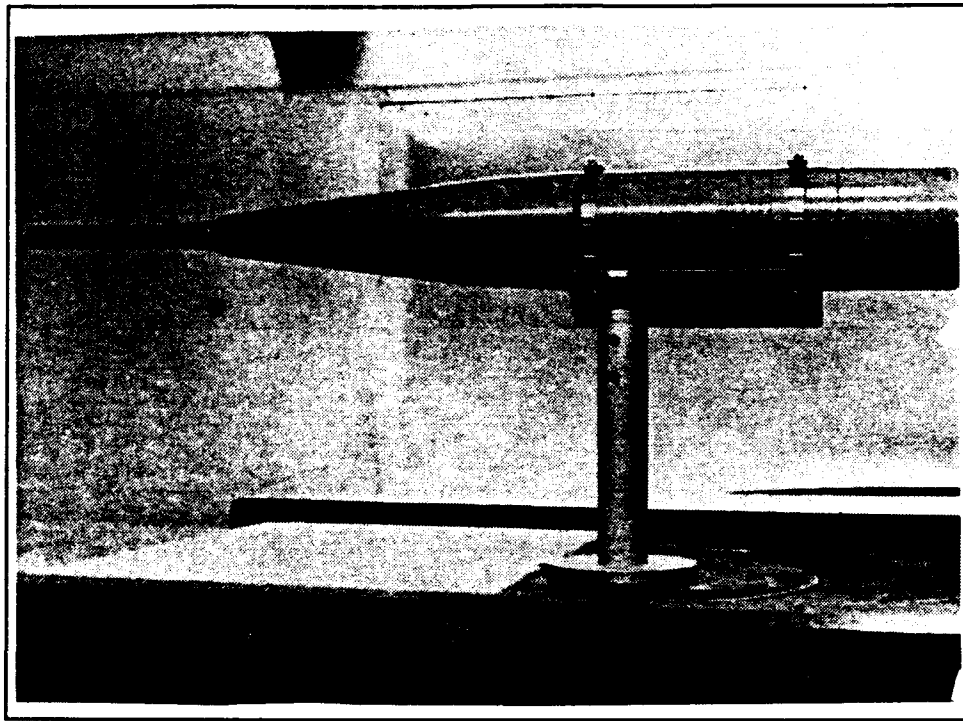


Figure 10. Calibration of SAIP (Volts/psia).

of an adequate range of possible flow impingement directions on an aircraft-mounted SAIP.



**Figure 11. NCA Mounting Assembly (side view).**

#### **4. Instrumentation**

The NCA was integrated with its instrumentation equipment by coupling the connector plug extending from the output side of the ADU on the test article with an external Fluke Model 8810A Digital Voltmeter (DVM) via a  $\pm 15$  volt power supply. The module containing the power supply (Figure 12) was designed to permit manual scanning of the four voltages output from the ADU corresponding to either static pressure, total pressure, angle-of-attack pressure or angle-of-sideslip pressure. The power supply housing

also accommodated sampling of the voltage corresponding to the differential pressure existing between the tunnel test section and ambient air outside of the tunnel.

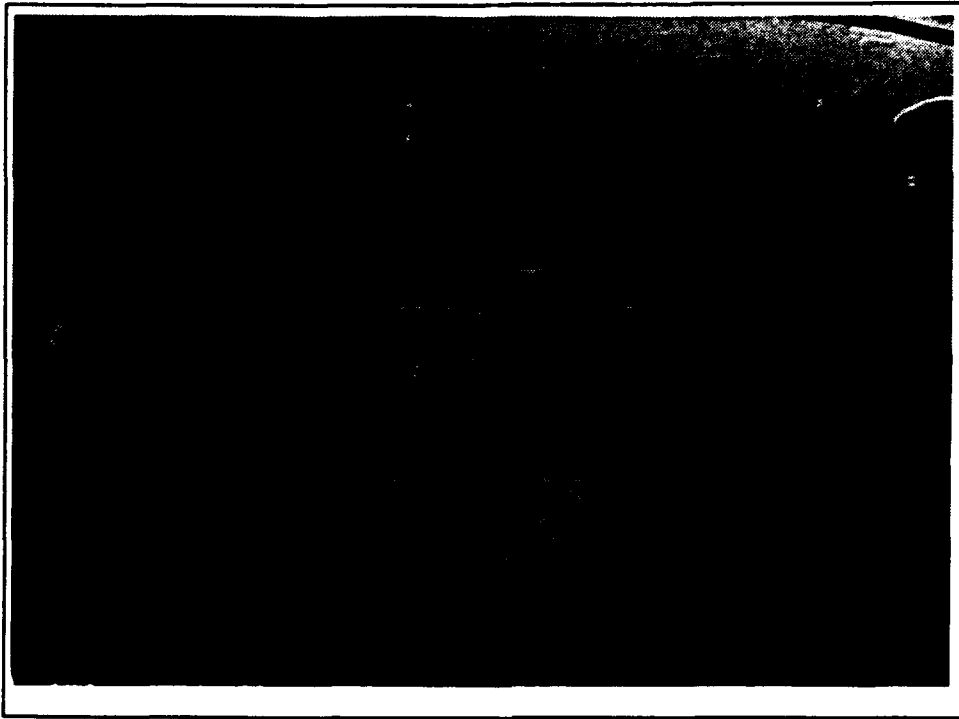


**Figure 12. Power Supply Module.**

While the design of the tunnel is such that the test section is maintained at a nominal pressure of one atmosphere, this pressure actually decreases during tunnel operation. The change in tunnel static pressure was measured with an inclined manometer and calculated to be 0.010 psia when  $V_{\infty}$  is 157.8 ft/sec. This change in pressure was combined with the pressure difference measured by the SAIP and plotted as  $\Delta P/P_{\infty}$  vs  $\theta$ .

## **B. WIND TUNNEL DATA**

### **1. Results Before Ground-Fix**

Original tests of the SAIP in the wind tunnel showed significant deviation in values of  $\Delta P$  when the angle- $\theta$  was rotated from  $-45^\circ$  to  $180^\circ$ . Specifications of  $\pm 0.0638$  psia were not being met. It was reported in previous work [Ref. 3:p. 91] that disconnecting various combinations of AOA, sideslip, and total pressure transducers produced pressure differences within specifications. However, voltages being read from the transducers through the digital voltmeter were approximately 0.5 volts, and specifications called for 5 volts.

Engineers from the Navy Standards Laboratory, Point Mugu, CA, reported identical results to those found by researchers at NPS. When  $\pm 15$  volts were applied to the SAIP from one power source, to give 30 volts, they observed an output of less than 0.5 volts from the static pressure transducer. Further analysis of SAIP manufacturer's specifications showed a requirement for + 15 volts to pin 8 of the ADU and - 15 volts to pin 6. When a single power source was used to provide 30 volts across the two pins, a low voltage output occurred. But, when two power sources were used, one producing + 15 volts and the other - 15 volts, the correct readings of 5.7 volts were obtained. This problem is commonly referred to as a "floating ground" as it is unknown whether the specific voltage requirements to each pin are being met even though the voltage across the pins is correct. Examination of the power source used on the SAIP when placed in the NPS wind tunnel revealed that we also suffered from a "floating ground."

Reconfiguration of the power source produced a static pressure transducer output in the specified range and allowed us to focus on the aerodynamics portion of the problem.

## 2. Data After Ground-Fix

Once it was established that the power requirements of the SAIP were being met, and the voltage output from transducers was increased by an order of magnitude, calibration curves were constructed allowing the conversion of  $\Delta$ Volts to  $\Delta P$  (Figure 10). The SAIP was again placed into the wind tunnel and voltage measurements taken at 13 cm H<sub>2</sub>O (157.8 ft/sec). The SAIP was rotated through angles of  $\theta$  ranging from - 45° to 180° and at each position the angle- $\phi$  was varied from - 20° to 20°. Voltages read directly from the voltmeter were compared to the voltage measured when tunnel velocity was not on and the  $\Delta$ Volts converted to  $\Delta P$ . It was observed that the size of the SAIP NCA caused measurable blockage in the test section of the NPS wind tunnel. A correction was applied to the measured  $\Delta P$  to correct the tunnel test section pressure to ambient pressure and a plot created of corrected  $\Delta P$  vs  $\theta$ . Figure 13 shows that rotation of the SAIP through any angle- $\theta$  has no effect on  $\Delta P$ .

Theta variations play a minor part in changing values of  $\Delta P$ , but Figure 13 does show a significant effect, caused by changes of the angle- $\phi$ . It was determined that the most useful way to observe a  $\phi$  dependence, and to check the theoretical model proposed for  $C_p$ , was to plot  $(P_s - P_\infty)/P_\infty$  vs  $\phi$ . Figure 13 data are already corrected for the underpressure of the tunnel with respect to the atmosphere.

The relationship between  $\frac{P_s - P_\infty}{P_\infty}$  and  $C_p$  is as follows:

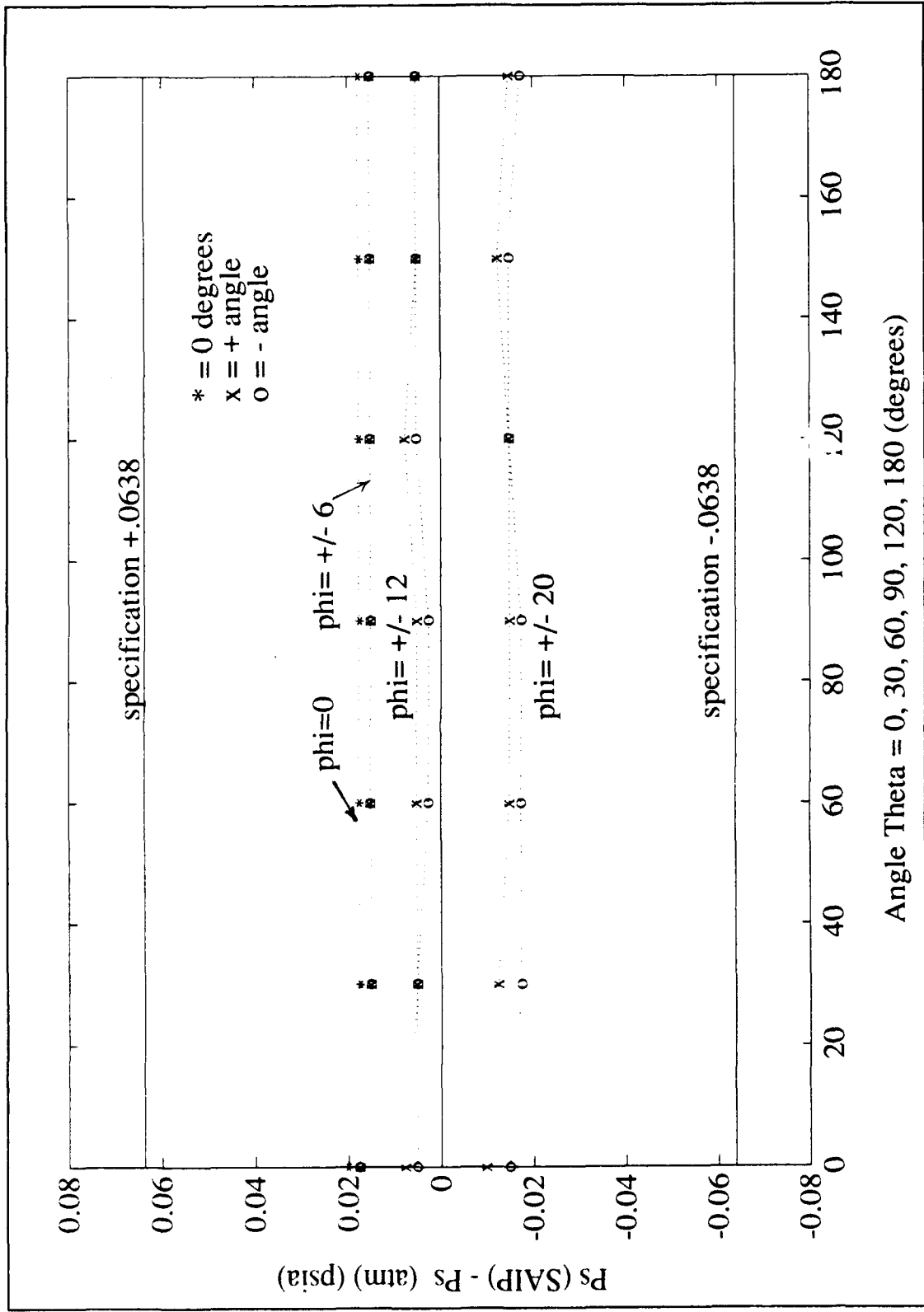


Figure 13. Pressure Difference of SAIP and Atmosphere.

$$\frac{P - P_{\infty}}{P_{\infty}} = \frac{q_{\infty}}{P_{\infty}} C_p \quad (22)$$

$$\frac{q_{\infty}}{P_{\infty}} = \frac{1}{2} \frac{\rho_{\infty} V_{\infty}^2}{P_{\infty}} = \frac{1}{2} \frac{\rho V_{\infty}^2}{\rho R T} \quad (23)$$

$$\frac{q_{\infty}}{P_{\infty}} = \frac{\gamma}{2} M_{\infty}^2 \quad (24)$$

$$\frac{P_s - P_{\infty}}{P_{\infty}} = \frac{\gamma}{2} M_{\infty}^2 C_p \quad (25)$$

Knowing  $M_{\infty}$  together with measurements of  $(P_s - P_{\infty})/P_{\infty}$  we can deduce values of  $C_p$  from wind tunnel data. These are actually  $C_{p0}$  because  $M_{\infty} < 0.3$ .

Data from wind tunnel testing were plotted (Figure 14) and a 3rd-order polynomial fit drawn through the average value of all measurements for a particular angle- $\phi$ . To this plot are overlaid values calculated using  $C_{p0}$  from Equation (8), where values of C2 are varied to give the best fit. Figure 14 also reveals that for  $\phi < 20^\circ$ , C2 affects the maximum value of  $C_p$ , but not the shape of the curve. In the second step of a two step curve fitting process C1 was increased from an initial value of 2.0 while holding C1=0.91. Figure 15 shows that the constant C1 impacts the shape of the curve when  $\phi$  is increased from  $0^\circ$ . Substitution of values for C1 and C2 which best fit experimental data into Equations (8) and (9) give the equivalent Equations (26) and (27).

$$C_{p0} = 1 - 2.4 \sin^2 \phi - 0.91 \cos^2 \phi \quad (26)$$

$$C_{p0} = 0.9 - 1.41 \sin^2 \phi \quad (27)$$

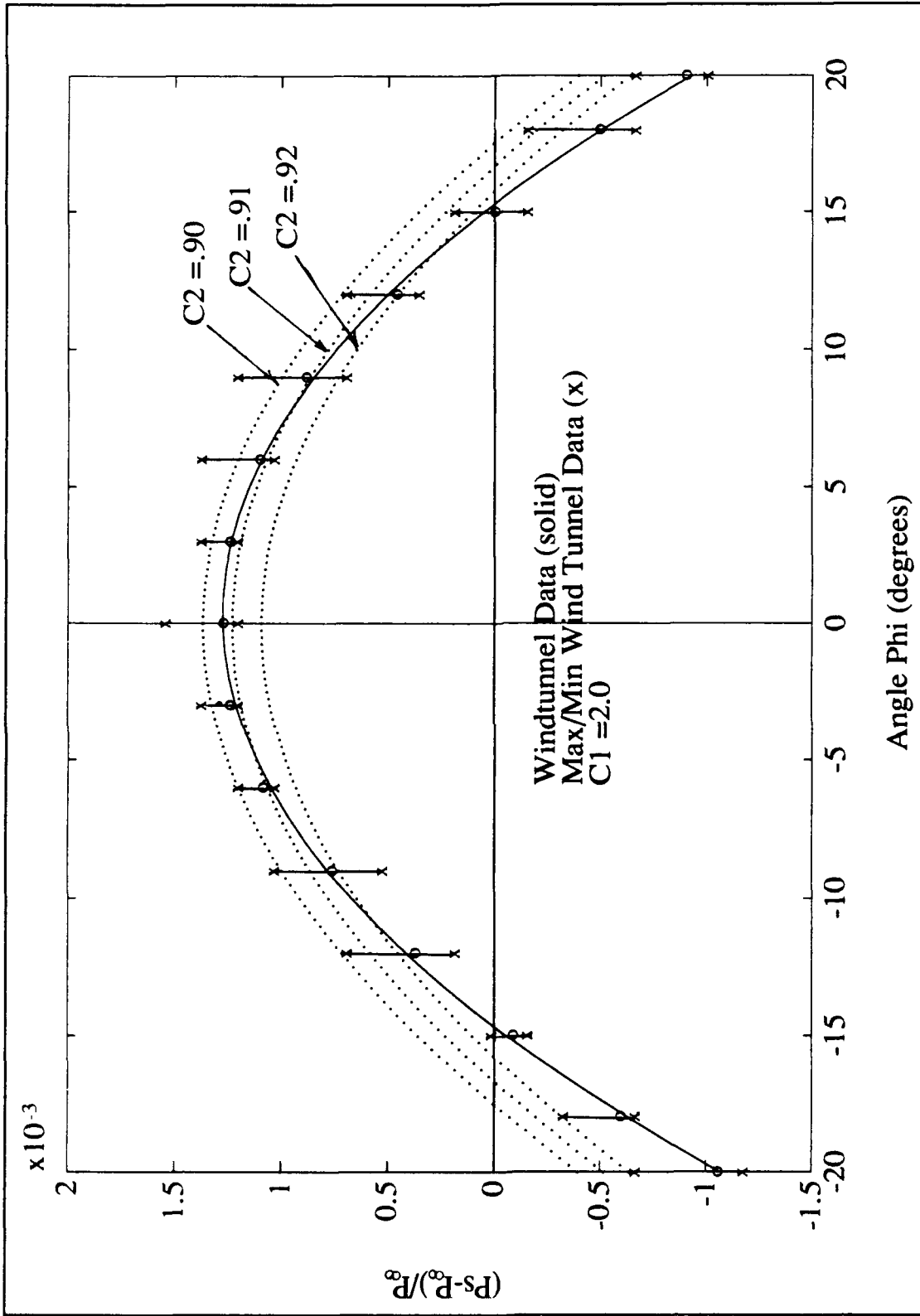


Figure 14. SAIP #0040; Wind Tunnel Data vs. Theory.

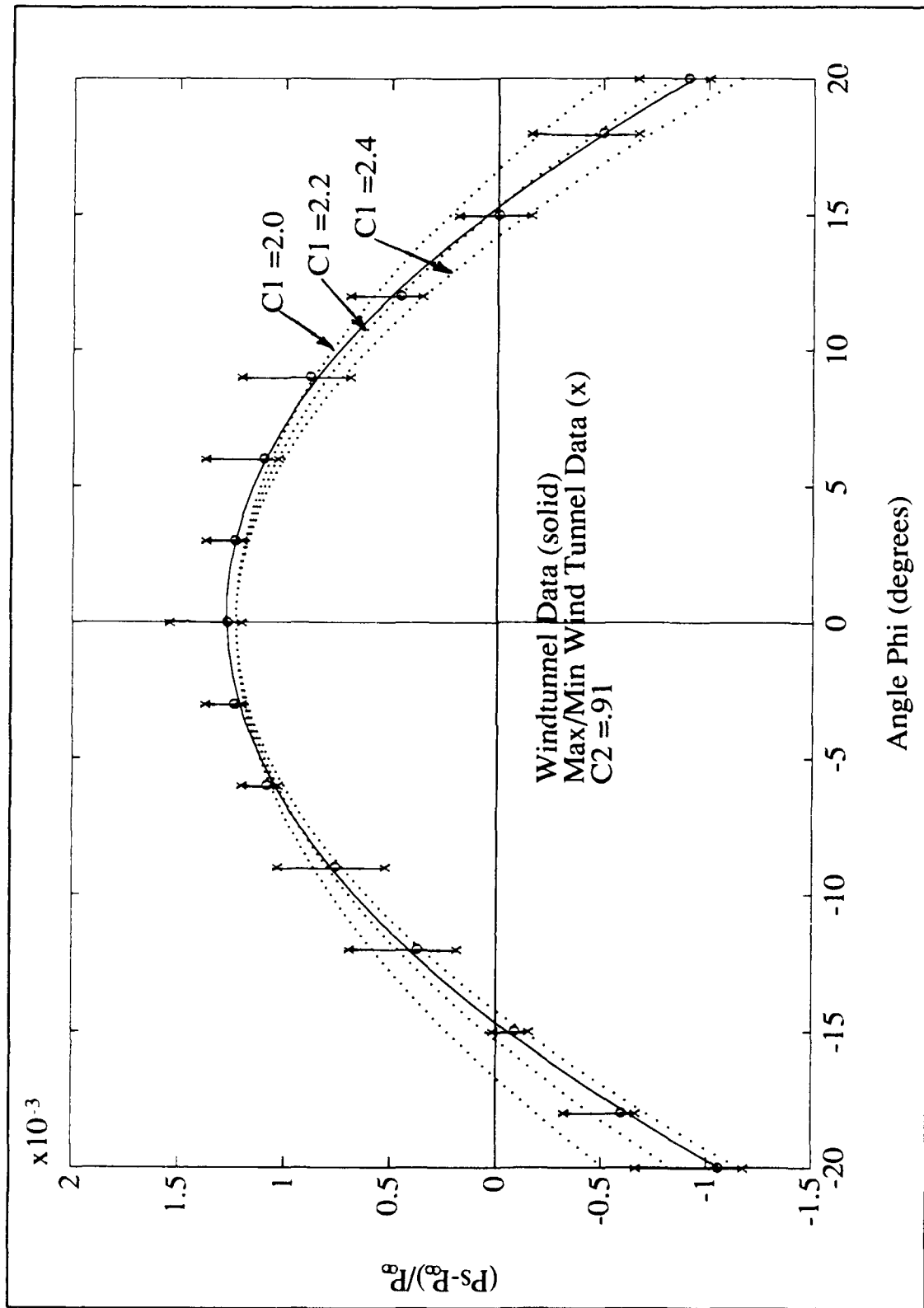


Figure 15. SAIP #0040; Wind Tunnel Data vs Theory.

Closer examination of Figure 15 reveals that, at small but significant values of  $\phi$ , an overpressure is occurring at the static pressure ports. This result seems contrary to expectations. It was felt that the flow velocity might increase around the hemispherical end of the probe. A simple application of Bernoulli's Equation reveals that a lower pressure would be expected on an infinite cylinder which is just opposite to what was observed in the wind tunnel.

If the SAIP is viewed in its entirety, i.e., as a large body with a static pressure probe in front, it is conceivable that the stagnation region created by this larger object will affect the measured static pressure and result in a positive  $C_p$  value. As the entire probe is rotated through an AOA greater than approximately  $14^\circ$ , the five-inch diameter body of the SAIP will have a decreasing influence on the probe and negative values of  $C_p$  are measured as the flow increases speed around the circular cylinder and hemisphere.

### **3. Elevation Defect ( $\Delta Z$ )**

Equation (18) can now be used to look at the effect on  $\Delta Z$  caused by changes in  $C_p$ . Values for  $\Delta Z$  have been calculated for Mach numbers ranging from 0.15 to 0.85 and angles- $\phi$  from  $0^\circ$  to  $16^\circ$  at an altitude of 10,000 feet (Figure 16). It was determined in the derivation of Equation (20) that the value computed for  $\Delta Z$  is not a direct function of the altitude  $Z$ . Therefore, Figure 16 uses 10,000 feet, as flight test data taken at that altitude are available for comparison. It is important to remember that as the host aircraft increases and decreases airspeed the AOA, and therefore the angle- $\phi$  seen by the SAIP, will change. Furthermore, it becomes evident that any misalignment of the probe when attached to the aircraft and/or wing buffet during flight will result in a deviation of

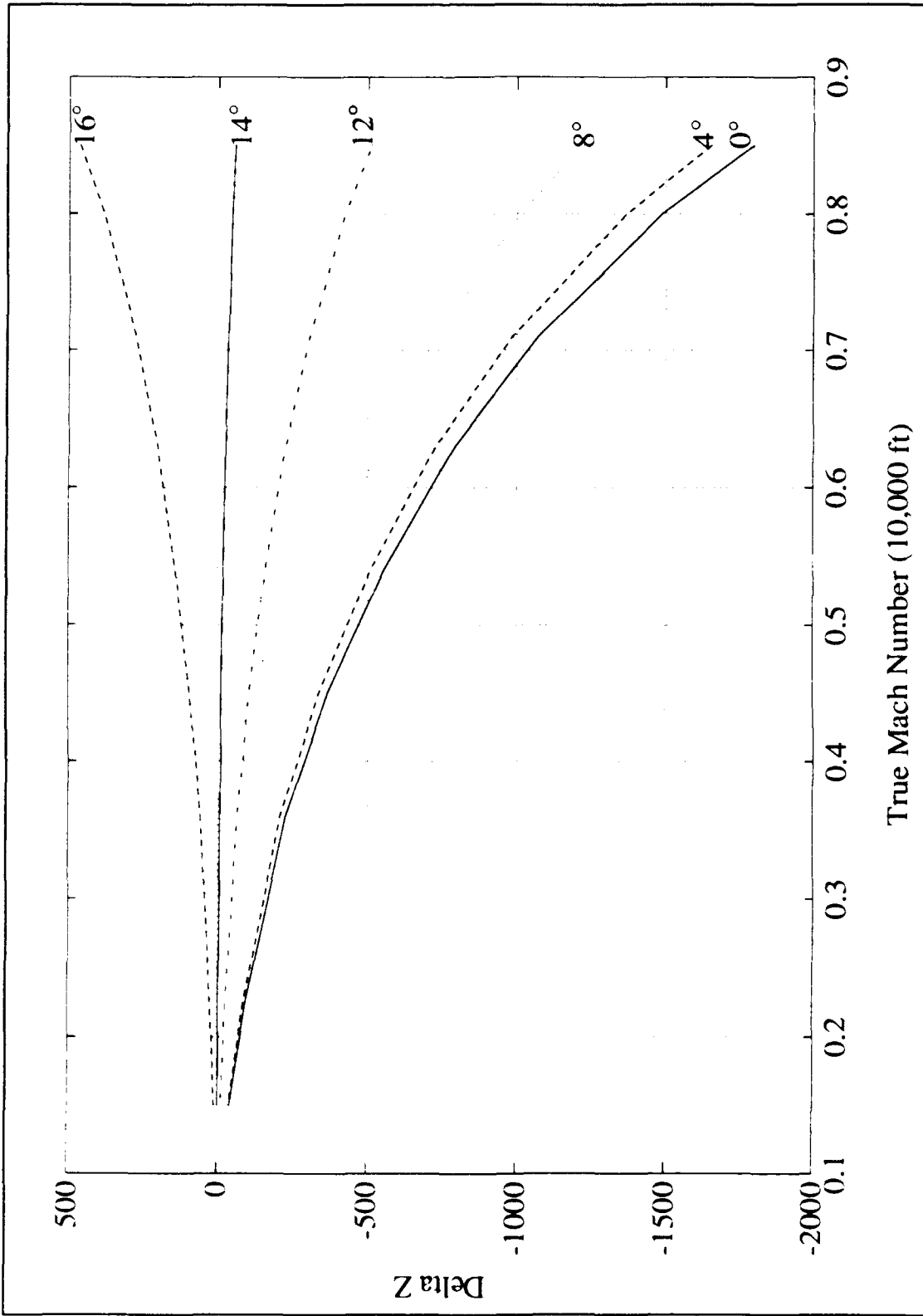


Figure 16. Converted Theoretical  $C_p$  to  $\Delta Z$  (feet).

altitude. A rough estimate of these errors alone could total  $\pm 3^\circ$  and represent a significant percentage of the altitude error since it has previously been determined that the A-6 aircraft should not exceed  $10.9^\circ$  AOA in flight. Limiting a discussion and analysis of the effect on  $\Delta Z$  of  $\phi$  and  $M_\infty$  to angles- $\phi$  less than  $15^\circ$  seems therefore appropriate.

When examining Figure 16 it must be noted that as the test aircraft increases Mach number the AOA transitions from a curve for a large AOA to a lower value of AOA. These decreases in AOA will also appear in Figure 15 as an increase in the value of  $C_p$ . The error computed for  $\Delta Z$  is a value that must be subtracted from the altitude  $Z$  used in Equation (18). In flight, the value computed for  $\Delta Z$  must be added or subtracted from the true altitude in order to obtain the altitude measured by the SAIP.

#### **4. Flow Visualization**

To validate that the integration of  $\theta$  from 0 to  $2\pi$  does indeed correspond to ideal flow, the SAIP was fitted with four rows of tufts encircling the probe just aft of the static pressure ports. The SAIP was then placed in the NPS wind tunnel and run at a speed of 13 cm  $H_2O$  (157.8 ft/sec). Photographs were taken at angles ranging from  $0^\circ$  to  $20^\circ$  (Figure 17) in order to observe the angle- $\phi$  where the flow begins to separate.

At an angle- $\phi$  less than  $5^\circ$  the flow was observed to remain attached and parallel to the longitudinal axis of the SAIP. At angles from  $5^\circ$  to  $10^\circ$  the flow begins to be affected by the flow over a circular cylinder to a greater extent, but remains attached around the entire circumference. The first signs of flow detachment occur between  $10^\circ$  to  $15^\circ$  and become increasingly more evident as the angle is increased to  $20^\circ$ . Therefore, as the SAIP will seldom encounter an AOA greater than  $15^\circ$  when flown aboard the A-6,

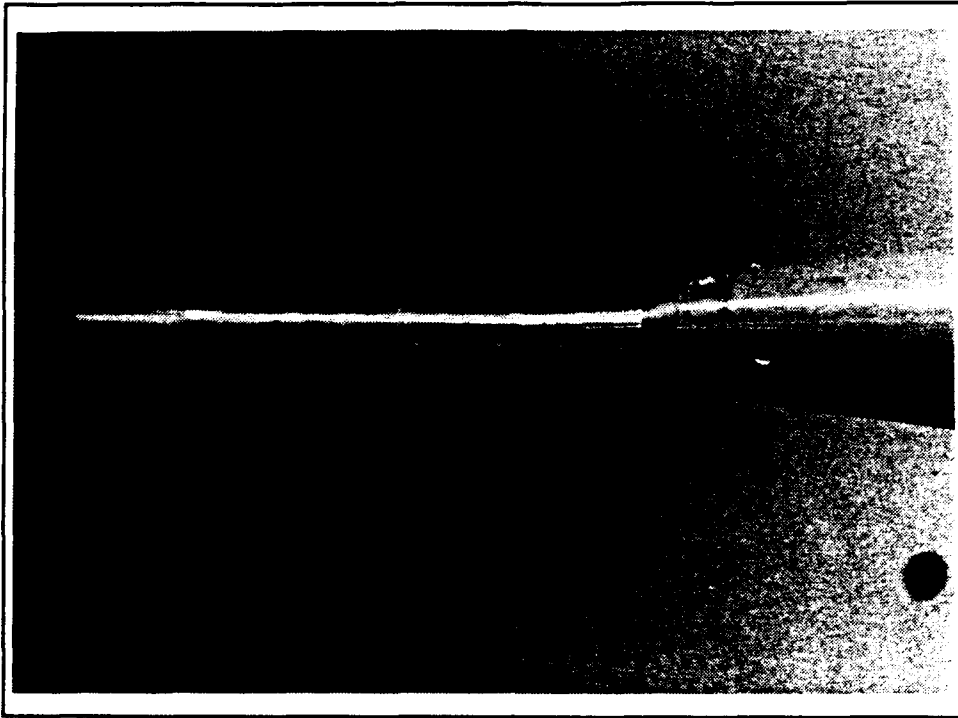


**Figure 17a. Photograph of SAIP and Tufts Where  $\phi = 0^\circ$ .**

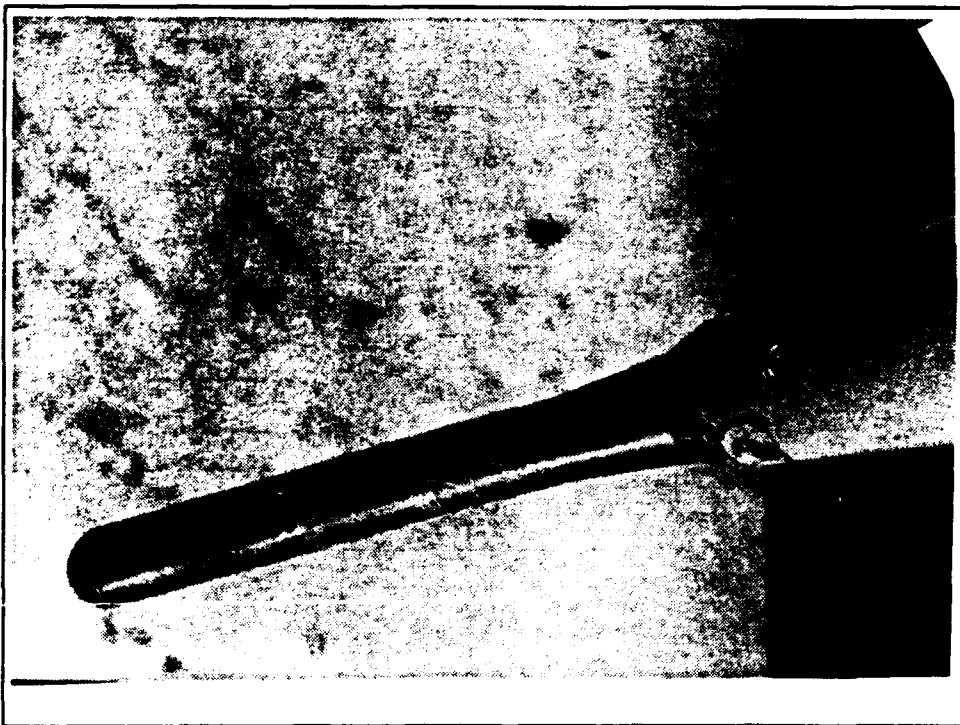


**Figure 17b. Photograph of SAIP and Tufts Where  $\phi = 15^\circ$ .**

integration of  $\theta$  from 0 to  $2\pi$  appears to be an accurate assumption in the derivation of Equation (8).

## IV. FLIGHT TEST

Examination of initial flight test data collected with the SAIP pod [Ref. 3:pp. 4-5] and subsequent finding of the A-6 Finboom-Altitude-Position-Error Correction chart [Ref. 4:p. 11-11] led us to confirm the conclusion that static-pressure-measurement errors may be caused by aerodynamic effects associated with all static pressure probes. Blockage effects, which can cause an overpressure at the static pressure ports (see section II.A), would vary in magnitude with each pitot static system configuration and thus account for the differences in the observed error  $\Delta Z$ .

### A. TACTS POD

#### 1. Description

To determine whether errors of equal magnitude would be read by a pod of similar design to the SAIP, but using a different system for altitude determination, flight tests were performed on the Navy's Tactical Aircrew Combat Training System (TACTS) pod (Figure 18) at the Naval Strike Warfare Center (NSWC), Fallon, NV.

The TACTS pod is nearly identical to the SAIP pod in both size and weight. In addition, the Air Data Sensor (ADS) used is functionally identical in both pods and is produced by the Rosemount Corporation, Burnville, MN. The ADS is capable of measuring the pressure required to compute indicated airspeed, true airspeed, Mach number, angle of attack, and angle of sideslip. The four pressures measured are impact

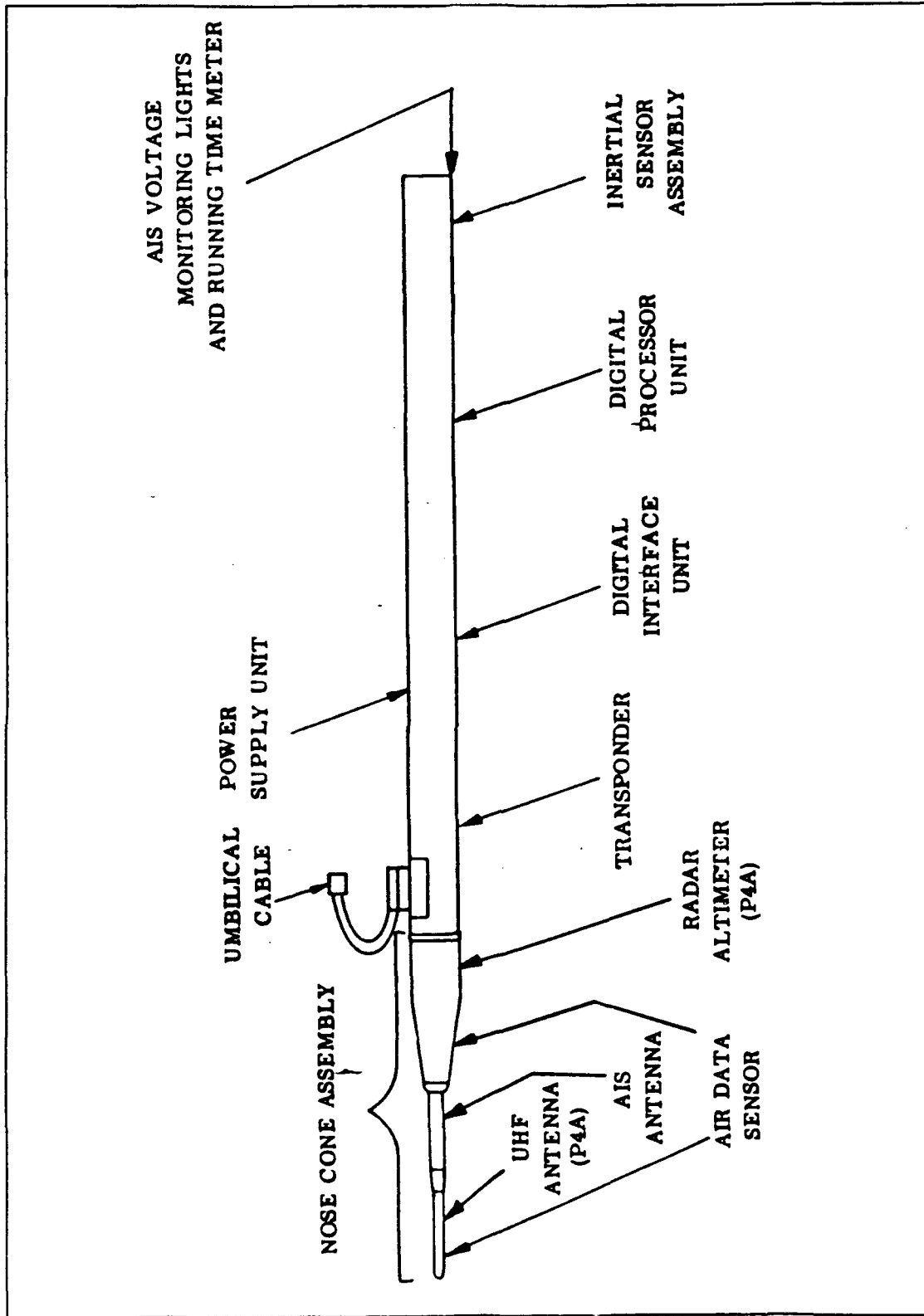


Figure 18. Tactical Aircrew Combat Training System (TACTS) Pod.

pressure, static pressure, and pressure related to angle of attack and angle of sideslip [Ref. 1]). The ADS consists of an Airflow Sensor Assembly (ASA) identical to that shown for the SAIP in Figure 9 and an Air Data Unit (ADU) that is functionally identical.

A major difference in the SAIP and TACTS pod ADA is that the former uses static pressure directly to compute altitude whereas the TACTS pod computes altitude using a sophisticated "multi-lateration" system. Multi-lateration requires the ability of three to seven receiving stations placed throughout a test area to measure the time difference of arrival of a signal generated by the TACTS pod to compute position, a restriction that the EATS system is trying to avoid in order to extend its operating range.

Both systems specify that "the altitude error in 50 percent of the track updates shall be less than the larger of 100 feet or three percent of the participant altitude [Ref. 1:p. 144]". A flight test of the TACTS pod was performed (courtesy of LT Brian Reeves, NSWC) to ascertain whether it met specifications.

## **2. TACTS Pod Flight Test**

An A-6 aircraft was configured with TACTS pods on station 2 and 4 (Figure 19) and stations 1, 3 and 5 were left empty. After take-off the aircraft climbed to 10,000 ft and conducted a wings-level acceleration from 250 to 480 KIAS followed by a deceleration to 250 KIAS. The aircrew maintained 10,000 ft by monitoring the barometric altimeter in the RESET mode. In the RESET mode, the altimeter displays altitude, corrected for position error, from the output of the Air Data Computer (ADC) altitude module [Ref. 4:p. 1-69].

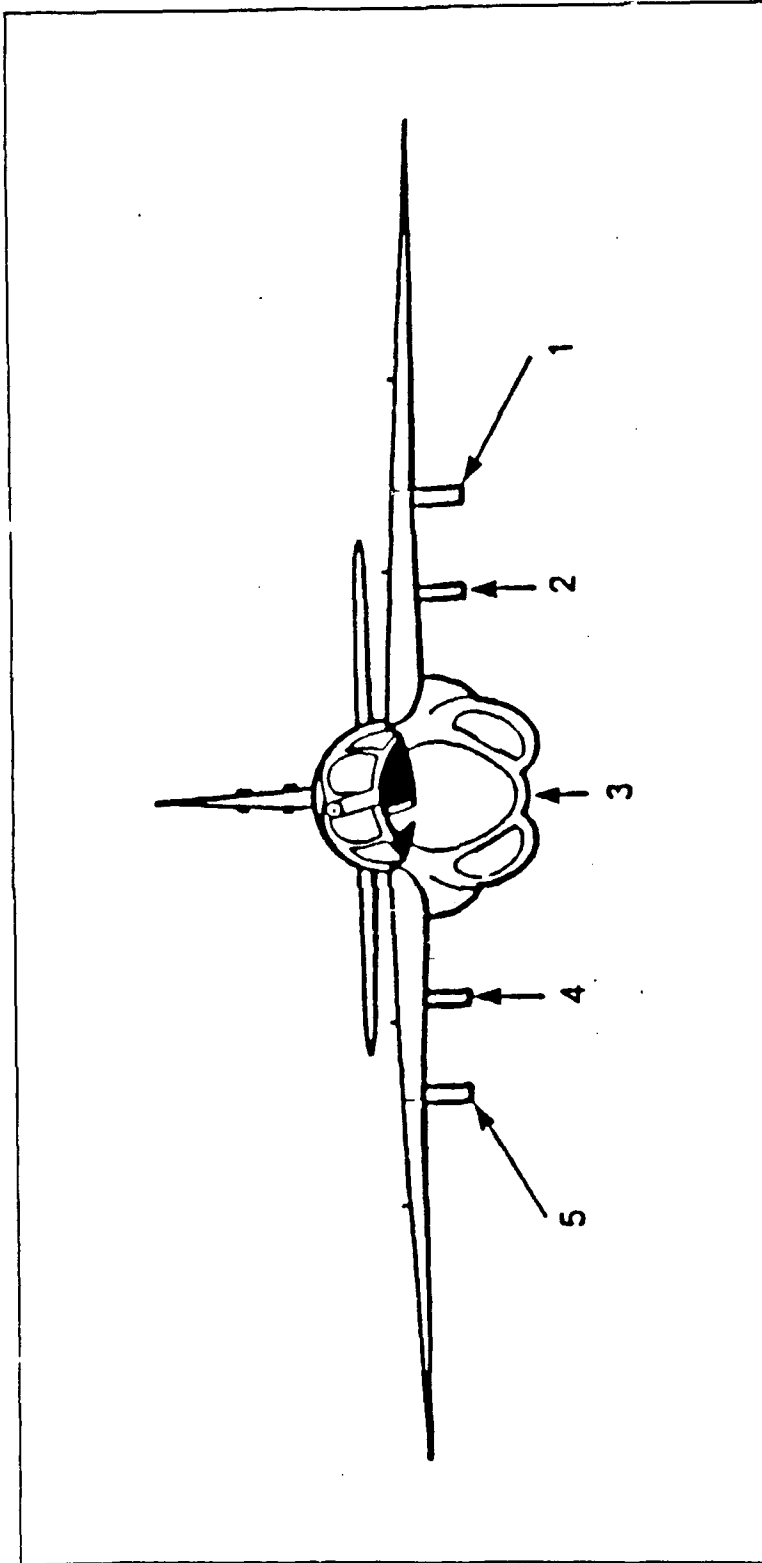


Figure 19. A-6 Aircraft and Wing Stations.

The aircrew collected data in flight and personnel located at the central receiving station recorded altitudes measured by the TACTS pods (Appendix B). The local NSWC elevation (3934 ft) prevented collection of data at 4,000 ft which could have been compared to that collected at Point Mugu, CA.

Figure 20 shows a plot of static pressure altitude versus indicated Mach number (IMN). The altitude difference observed between corrected and uncorrected static pressure altitude correlates well to the Altimeter Position Error Correction chart shown in the A-6 NATOPS manual. The position error chart shows that 650 ft must be added to the barometric altimeter in STANDBY mode to give aircraft true altitude and this test produced a  $\Delta Z$  of 500 ft. This lower altitude measurement with increasing Mach number, computed using a static pressure probe located on the aircraft vertical stabilizer, could be caused by aerodynamic effects similar to those postulated to occur on the SAIP probe.

Figure 21 shows a plot of altitudes determined by the two TACTS pods versus IMN. Of particular note is the fact that the pod altitudes reported did not deviate more than 287 ft from that computed by the A-6 aircraft ADC. This altitude error is within the specification limits of the TACTS pod. It is thus apparent that their multi-lateration system for altitude measurement is a viable alternative to static pressure measurement when an adequate number of receiving stations can be used.

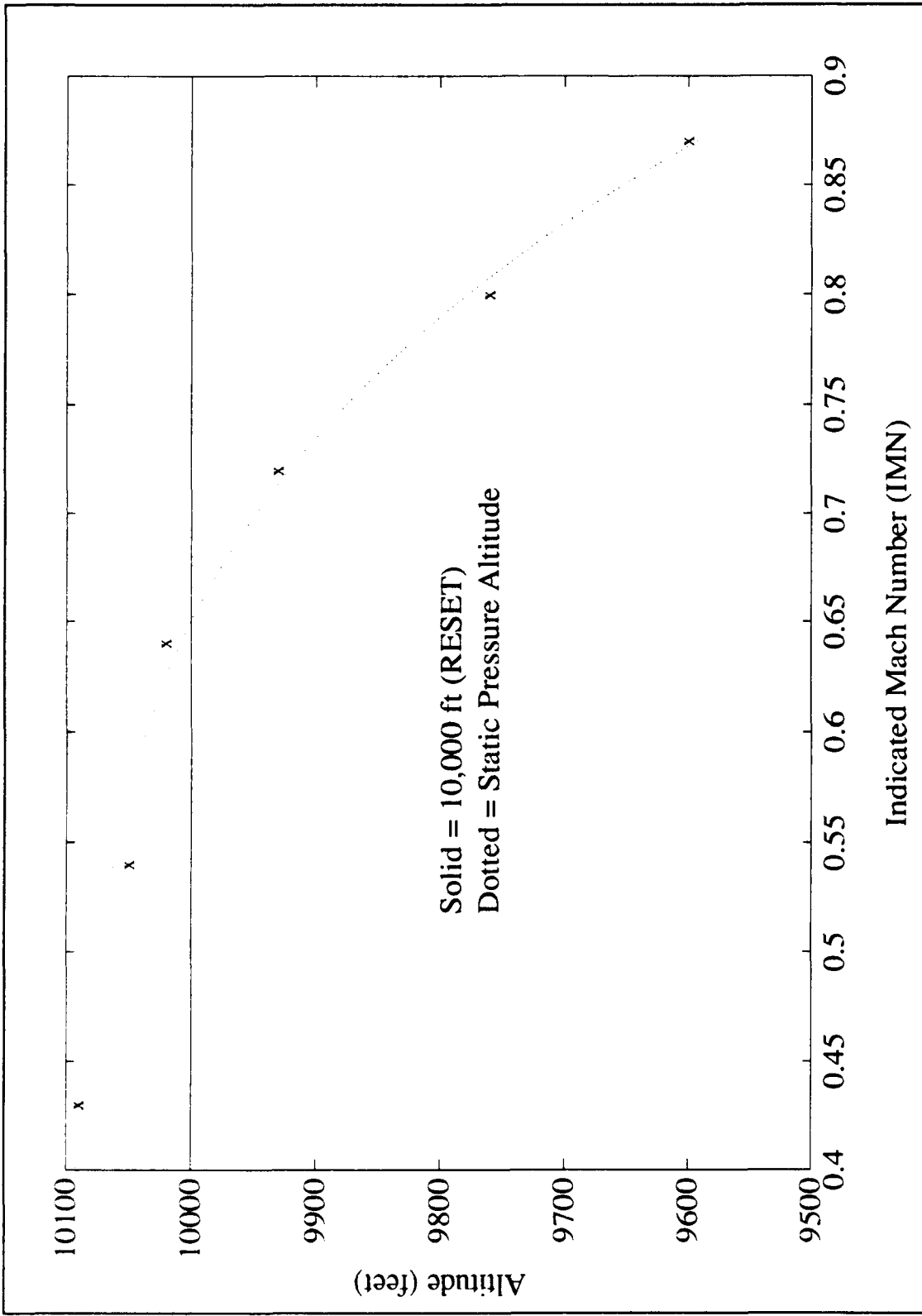


Figure 20. Static Pressure Altitude Versus Indicated Mach Number.

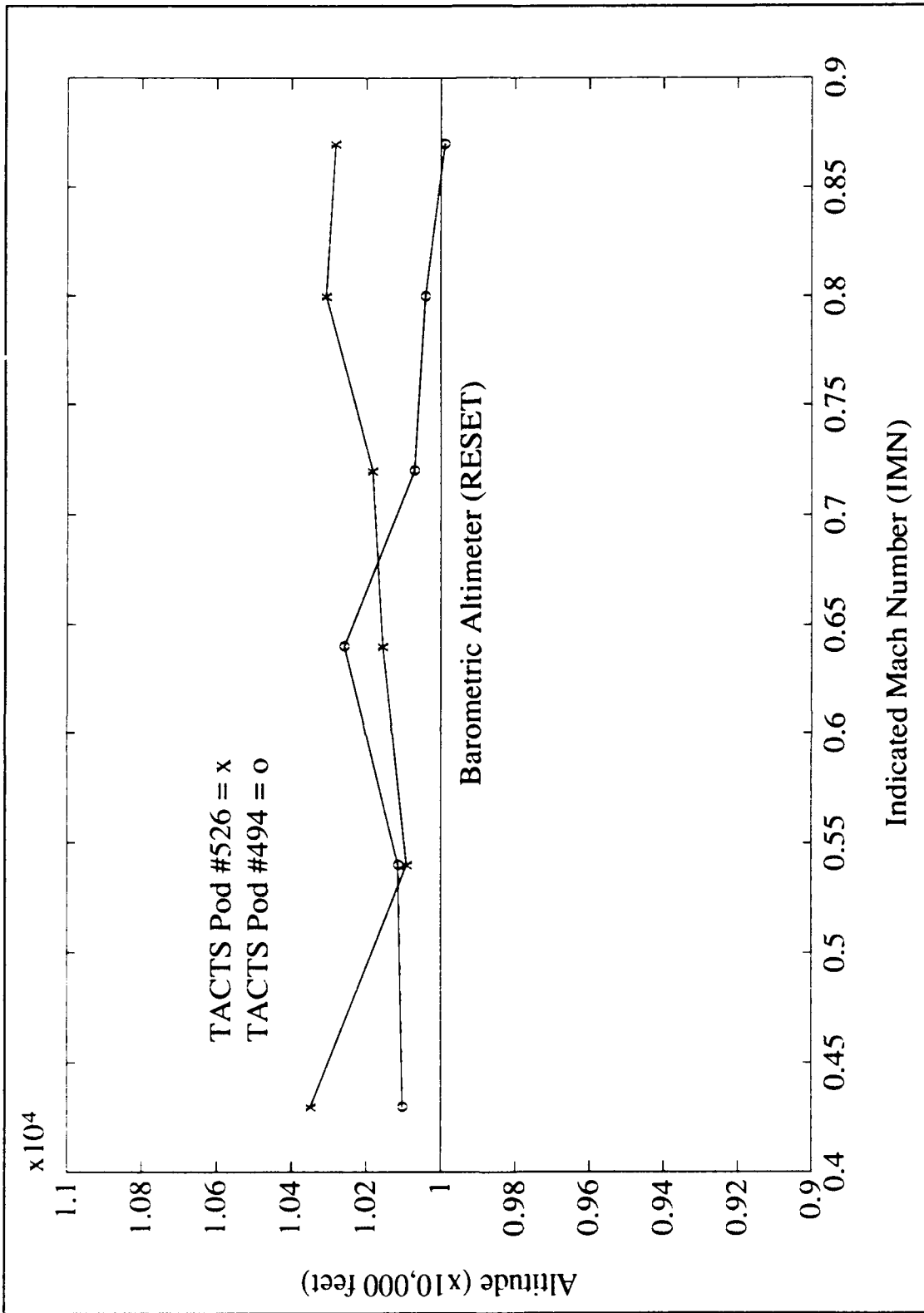


Figure 21. TACTS Pod Altitude Determination (10,000 ft).

## B. SAIP POD

### 1. Flight Test Description

Flight testing of the SAIP pod would be used to validate the algorithm derived for the computation of  $\Delta Z$ . Equation (20) shows a dependence on  $\Delta Z$  of  $C_{po}$ , modeled by Equation (27), and  $V_\infty$ .  $C_{po}$  must be corrected for compressibility at Mach numbers greater than about 0.3, thereby making  $C_p$  a function of both the angle- $\phi$  and  $M_\infty$ . Flight tests must try to distinguish effects on  $\Delta Z$  from all the factors leading to these altitude errors.

It is extremely important that an accurate measure of aircraft altitude be recorded so that the output of the SAIP pods may be compared for the study of  $\Delta Z$ . The aircrew should maintain altitudes below 5,000 ft by using the A-6 radar altimeter. The most accurate method of flying a constant altitude above 5,000 ft will be to use the barometric altimeter in RESET mode where static pressure is corrected by the ADC for altimeter position error. Range personnel at PMTC are also able to use radar triangulation for aircraft operating within the EATS range to give a second source of aircraft position and altitude.

Once airborne, the aircraft should fly a minimum of three different flight profiles at altitudes of 4,000 and 10,000 ft. The first profile is a wings-level acceleration at speeds ranging from 250 to 500 KIAS immediately followed by a deceleration to 250 KIAS. Airspeed, indicated Mach number (IMN), angle of attack (AOA), and barometric altimeter reading in both the STANDBY and RESET mode should be recorded by the aircrew. Flight data computed by the SAIP pods will be obtained by EATS range

personnel. If the aircraft AOA was known for each Mach number it would be possible to plot the values of  $\Delta Z$  computed by our model, shown in Figure 16, with values of  $\Delta Z$  obtained from SAIP altitude determination.

The second and third profiles flown should examine the effects of changes in  $\phi$  and  $V_{\infty}$  separately. Isolation of  $\phi$  would be accomplished by flying constant airspeed, level turns, and increasing the angle- $\phi$  by applying "g"-loads to the aircraft. At each angle- $\phi$  aircraft instrumentations, as well as SAIP data, should be recorded. Aircrew must ensure that "g"-load limitations are not exceeded for the aircraft. Furthermore, the airspeed chosen for this test should allow the largest possible variation in  $\phi$ . Initial examination of A-6 turn performance charts suggest that an upper value of 0.62 IMN (350 KIAS at 10,000 ft) would meet these limitations.

The study of  $V_{\infty}$  effect on  $\Delta Z$  would also involve level turns, but whereas the former test varied  $\phi$  as airspeed was held constant, this test would vary airspeed and perform turns under a constant AOA. The AOA chosen for this test should be such that a maximum velocity range can be examined. Aircrew must vary the aircraft angle-of-bank as  $M_{\infty}$  changes to maintain altitude and fly the same AOA. Also, if too large an AOA is chosen the aircraft will not be able to sustain a steady airspeed in the turns. Discussion with A-6 pilots at Point Mugu indicated that the optimum AOA for this test would be either 16 or 18 "units."

## **2. Test Results**

After extensive coordination with engineers at Point Mugu, a flight test was scheduled for 9 August 1991. A detailed test plan was drafted (Appendix C) which

incorporated the three phases of flight discussed in VI.B.1. Unfortunately, when power was applied to the aircraft the SAIP pods located on aircraft wing stations 1 and 5 were found to be inoperative. Initial reports from Point Mugu are that a "current overload" caused the AC/DC power supply unit within the SAIP to malfunction. This power supply unit converts the aircraft 115 Vac, 400 Hz power at the LAU-7A launcher connection to regulate dc voltages required by the DPU/DIU and the Air Data System [Ref. 1:p. 78]. The inability to replace the power supply with stock on hand caused the test cancellation and the aircraft did not fly that day.

For purposes of comparison, flight data collected from an earlier test [Ref. 2], and given in Appendix D, are examined with respect to our model of  $\Delta Z$  for the SAIP (Equation 20). Figure 22 shows a plot of  $\Delta Z$  for the four SAIP pods tested versus true Mach number. True airspeed (TAS) reported by the SAIP was converted to true Mach number using airspeed conversion tables found in the A-6 NATOPS. Figure 22 depicts only a plot where  $\phi=0^\circ$  as changes in angle- $\phi$  with Mach number are not available in the literature and must be recorded during future flight tests.

Deviation of computed  $\Delta Z$  with flight test data are expected as our model is accurate only to Mach numbers of approximately 0.7 due to limitation of the Göthert compressibility correction. Safety of flight restricts airspeeds at 10,000 ft to 250 KIAS and above.

The Göthert compressibility correction which was used to correct our model of the SAIP (Equation 8) assumed the probe to have the same properties as a thin ellipsoid of revolution where  $\delta=1/5$  (Figure 22). Figure 23 shows a plot of the SAIP

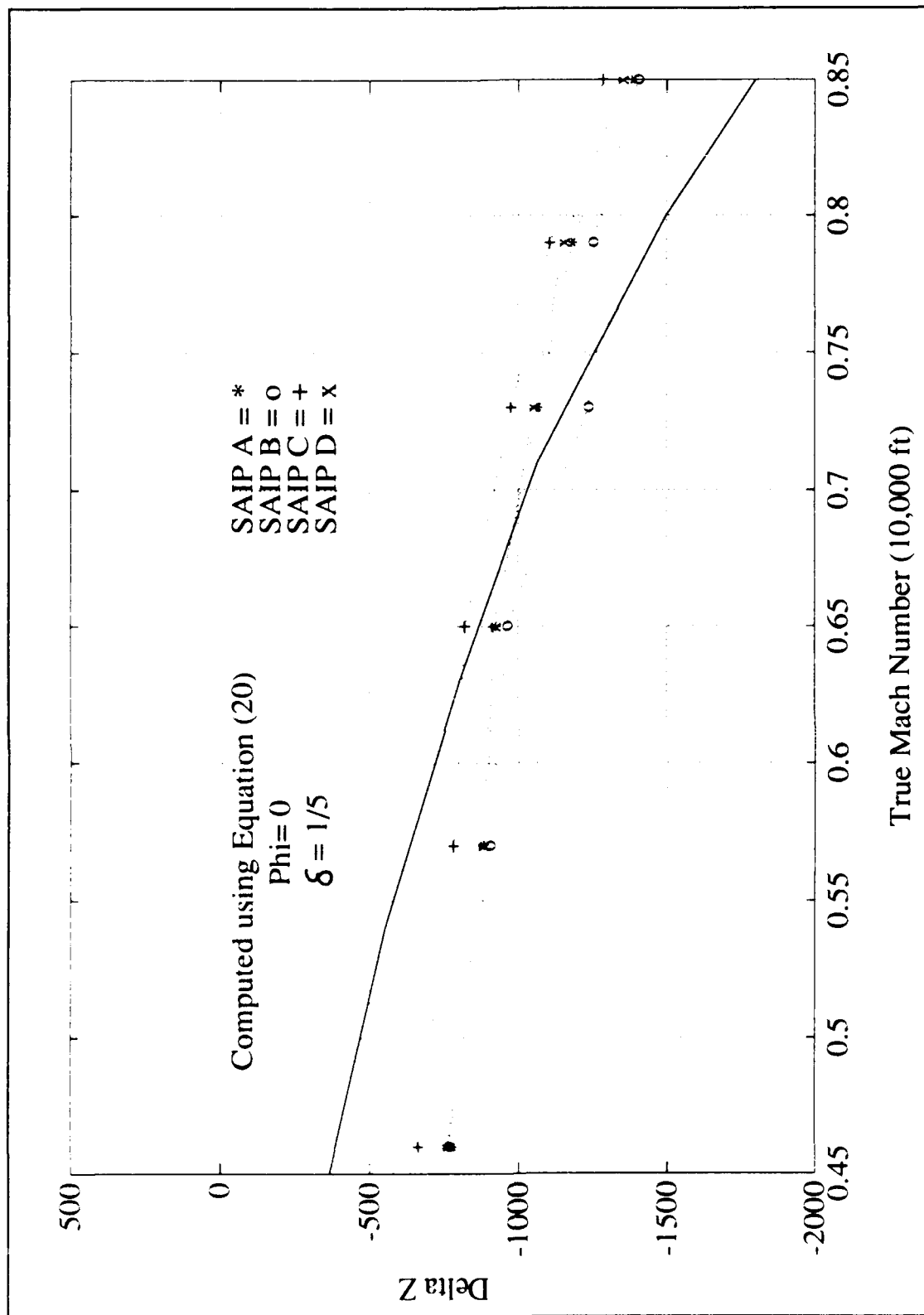


Figure 22. Altitude Error Determination ( $\Delta Z$ ). Comparison of Equation (20) to SAIP Flight Test Data.

model where  $\delta=1/15$ . As theoretical calculations of  $\Delta Z$  more closely approximate what is observed in actual flight, it has become apparent that a more detailed analysis of the compressibility correction is necessary.

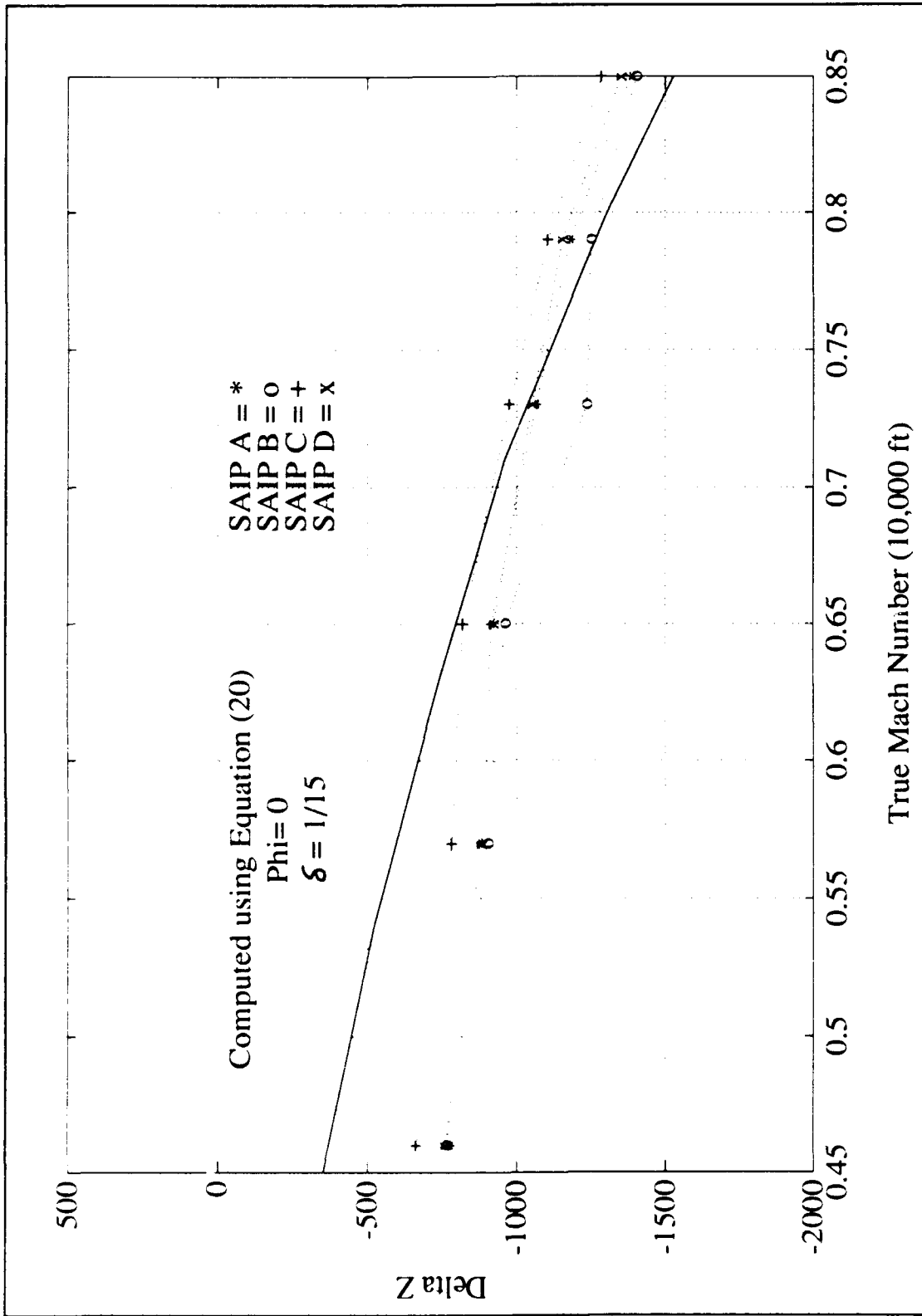


Figure 23. Altitude Error Determination. Comparison of Equation (20) to SAIP Flight Test Data.

## V. CONCLUSIONS AND RECOMMENDATIONS

### A. CONCLUSIONS

It was initially felt that the altitude errors reported by the SAIP were the result of an electrical design error within the ADU. Subsequent study of the power supply unit revealed that an ambiguous grounding requirement in the SAIP specification had been misinterpreted. After correcting this "floating ground", efforts were redirected to a study of the aerodynamics effecting SAIP altitude measurement. Utilizing a combination of theoretical analysis and wind tunnel data, an algorithm has been derived which provides for computation of the error  $\Delta Z$  that might be observed in flight. Initial data from wind tunnel testing, combined with information published in the Naval Air Training Operating Procedures Standardization (NATOPS) manual for A-6 aircraft and conversations with experts, indicate that a portion of the error in altitude measurement ( $\Delta Z$ ) is due to aerodynamic factors and is endemic to current models of static pressure probes used on Naval aircraft.

A number of conclusions from this study have been established:

#### 1. Analysis

- The SAIP probe may be partially modeled using elementary pressure distribution equations for a circular cylinder and hemisphere. The algorithm shows a dependence on the angle- $\phi$  (mostly AOA) and the angle- $\theta$  about the circular cylinder. However, static flow measurements average out the  $\theta$ -distribution from the 12 static pressure ports located about the circumference of the probe.

- The  $C_p$  measured for the SAIP in NPS low-speed wind tunnel testing showed the constants of the derived algorithm for  $C_p$  to be somewhat different than those given for ideal shapes. A two-step curve fitting process was used to determine the constants which best fit test data.

$$C_{p_{po}} = 1 - 2.4\sin^2\phi - 0.91\cos^2\phi \quad (26)$$

- The Göthert Compressibility Correction for a thin ellipsoid of revolution is used to correct theoretical calculations of  $C_p$  for affects due to compressibility. All wind tunnel testing was done at low speeds (<0.3 Mach number), requiring the utilization of this compressibility correction to compare our results with flight data.
- The error  $\Delta Z$  is a function of  $C_p$  and  $V_\infty$ . In addition, the derivation of  $C_p$  from elementary equations shows it to be a function of  $\phi$  and  $M_\infty$ . Therefore, increases in  $M_\infty$  increase  $\Delta Z$  in a two-fold manner, by decreasing  $\phi$  and increasing  $V_\infty$ .

$$\Delta Z \equiv \frac{-C_p V_\infty^2}{2g} \quad (20)$$

## 2. Wind Tunnel Tests

- Wind tunnel data were collected for angles ranging from  $\pm 20^\circ$ , an angle at least  $5^\circ$  greater than that which will ever be experienced by the SAIP when flown aboard the A-6 aircraft. Flow visualization studies indicated that the flow remains attached at angles <10-15 $^\circ$ .
- Rotation of the SAIP through an angle- $\theta$  about the longitudinal axis has no effect on the static pressure measurement. However, changing the AOA ( $\phi$ ) produced significant changes in  $\Delta P$ . When the angle- $\phi$  is less than  $14^\circ$  an overpressure occurs at the static ports which reaches a maximum when  $\phi=0$ . As  $\phi$  increases beyond  $14^\circ$ ,  $C_p$  becomes negative.
- It is apparent that the five-inch diameter body of the SAIP affects measurements read at the static ports located only six inches in front of the main five-inch diameter body. The overpressure produced at the static ports when the angle- $\phi$  is small may be viewed as a progression of the stagnation region toward the static and below.

### 3. Flight Testing

- Flight tests of the Tactical Aircrew Combat Training Systems (TACTS) pod, which utilizes an identical Airflow Sensor Assembly (ASA) as the SAIP pod, shows that their altitude determination meets system specifications. However, whereas the SAIP pod uses only static pressure to determine altitude, the TACTS pod utilizes a more sophisticated "multi-lateration" system.
- A plot of the error  $\Delta Z$ , reported by four SAIP pods flown at 10,000 ft as Mach number increased from 0.46 to 0.85, shows  $\Delta Z$  increasing from 700 ft to 1300 ft. A calculation of  $\Delta Z$  using the model shows an increase of 400 ft to 1500 ft over the same range in Mach number.
- Measurement of changes in  $\phi$  with variations in  $V_\infty$ , and a more accurate determination of the constant  $\delta$  in the Göthert Correction should produce a more accurate curve fit. The value for  $\delta$ , the ellipsoid thickness ratio, in the compressibility correction is most important for fitting the curve at high Mach numbers. In contrast, at low Mach numbers the angle- $\phi$  affects  $\Delta Z$  to a greater extent.

### B. RECOMMENDATIONS

Recommendations for achieving an accurate SAIP altitude determination capability are suggested as follows:

- The ASA should be tested in the NPS low-speed wind tunnel independent of the five-inch diameter body of the SAIP to determine if the ASA by itself accurately measures static pressure.
- Low speed wind tunnel testing of the entire SAIP with the antennas attached should be performed to determine the effect they have on the measurement of  $\Delta P$  and subsequent calculation of  $\Delta Z$  using the proposed model for  $C_p$ .
- Evaluation of the Göthert Compressibility Correction modeling the SAIP as a thin ellipsoid of revolution needs to be examined in greater detail. It may be possible to continue using this correction if a more accurate determination of  $\delta$  can be determined. However, it may be advisable to explore the derivation of a

compressibility correction which uses a shape which more closely resembles that of the SAIP.

- Future flight tests need to be performed which isolate the effect of  $\phi$  and  $V_\infty$  on  $\Delta Z$  separately. These tests must also include an accurate measure of aircraft altitude so that the altitude reported by the SAIP pod can be compared for a true  $\Delta Z$ .
- A study of the pressure distribution about the SAIP should be undertaken which utilizes computer aided modeling. Ideally, a two or three-dimensional panel method would be utilized to explore changes in  $\phi$  and  $V_\infty$  on pressure distribution.
- If and when it is determined that an overpressure occurs at the static ports due to blockage created by the afterbody of the SAIP, design recommendations should be made that place the static ports in a position which measures the true static pressure.

**APPENDIX A**  
**NCA WIND TUNNEL TEST DATA ( $\Delta$  VOLTS UNCORRECTED)**

THETA (degrees)	PHI (degrees)						
	-20	-18	-15	-12	-9	-6	-3
-45	-0.009	-0.007	-0.005	-0.001	.001	.002	.003
-30	-0.011	-0.008	-0.005	-0.003	.000	.002	.003
-15	-0.011	-0.009	-0.005	-0.002	.0000	.002	.002
0	-0.011	-0.008	-0.006	-0.003	-0.001	.002	.002
15	-0.010	-0.009	-0.005	-0.003	-0.001	.001	.002
30	-0.012	-0.009	-0.006	-0.003	-0.001	.001	.002
45	-0.012	-0.009	-0.006	-0.003	-0.001	.001	.002
60	-0.012	-0.009	-0.006	-0.004	-0.001	.001	.002
75	-0.011	-0.009	-0.006	-0.003	-0.001	.001	.002
90	-0.012	-0.009	-0.006	-0.004	-0.002	.001	.002
105	-0.010	-0.008	-0.005	-0.002	.000	.002	.003
120	-0.011	-0.008	-0.006	-0.003	-0.001	.001	.002
135	-0.012	-0.009	-0.006	-0.003	-0.001	.001	.002
150	-0.011	-0.009	-0.006	-0.003	-0.001	.001	.002
165	-0.012	-0.009	-0.005	-0.003	.000	.001	.002
180	-0.012	-0.009	-0.006	-0.003	-0.001	.001	.002

	PHI (degrees)							
	0	3	6	9	12	15	18	20
-45	.004	.003	.002	.001	-.001	-.004	-.007	-.009
-30	.003	.002	.002	.001	-.002	-.005	-.008	-.011
-15	.003	.003	.002	.001	-.002	-.004	-.006	-.010
0	.003	.002	.002	.001	-.002	-.004	-.007	-.090
15	.003	.002	.002	.000	-.002	-.006	-.008	-.011
30	.002	.002	.001	.000	-.003	-.005	-.008	-.010
45	.002	.002	.001	.000	-.003	-.006	-.009	-.011
60	.002	.002	.001	-.001	-.003	-.005	-.009	-.011
75	.002	.002	.001	-.001	-.002	-.005	-.008	-.011
90	.002	.002	.001	.000	-.003	-.006	-.009	-.011
105	.003	.003	.003	.002	-.002	-.004	-.007	-.009
120	.002	.002	.001	.000	-.002	-.006	-.009	-.011
135	.002	.002	.001	-.001	-.003	-.006	-.009	-.011
150	.002	.002	.001	.000	-.003	-.005	-.007	-.010
165	.002	.002	.001	.000	-.003	-.006	-.009	-.011
180	.002	.002	.001	-.001	-.003	-.005	-.008	-.011

**APPENDIX B  
TACTS POD FLIGHT TEST DATA**

**Station 2      TACTS POD #494**  
**Station 4      TACTS POD #526**

IAS	AIRCRAFT			TACTS POD	
	IMN	RESET	STBY	#526	#494
250	---	10K	10090	10349	10103
300	.54	10K	10050	10092	10115
350	.64	10K	10020	10156	10259
400	.72	10K	9930	10183	10071
450	.80	10K	9760	10307	10041
480	.87	10K	9600	10282	9989
450	.80	10K	9850	10203	10030
400	.73	10K	9930	10307	10101
350	.67	10K	9970	10275	10260
300	.56	10K	10040	10241	10274
250	---	10K	10090	10287	10275

**APPENDIX C  
TEST PLAN**

The Operations Director should use the following as a guide when communicating with the aircrew to ensure all vital data is collected.

\* Once the aircraft is established outbound and ready to perform the test, all recording equipment should be turned on.

\*\* Positive communications must be established with the aircrew.

\*\*\* An accurate time should be recorded of each "hack" by personnel on the ground (i.e. NPS and Mr. Frankhauser)

AIRCREW KNEEBOARD CARD #1

Test #1            A-6E  
Temp \_\_\_\_ (C of F)

SET-UP

- 1) Inbound leg of racetrack
- 2) Establish 250 KIAS, 4K (rad alt)
- 3) Report "established \_\_\_\_ kts, hack"  
at each airspeed
- 4) Record data

ALTITUDE

<u>KIAS</u>	<u>AOA</u>	<u>IMN</u>	<u>STBY</u>	<u>RESET</u>	<u>RADALT</u>	<u>TAS</u>	<u>PPA</u>
250					4k		
300					4k		
350					4k		
400					4k		
450					4k		
500					4k		

- 5) Slow to 350 KIAS
- 6) Turn outbound 3 G's, 350 KIAS
- 7) Report "established in turn, hack"
- 8) Record data

<u>KIAS</u>	<u>AOA</u>	<u>IMN</u>	<u>G's</u>	<u>RADALT</u>
350			3	4K

AIRCREW KNEEBOARD CARD #2

Test #2            A-6E

Temp \_\_\_\_\_(C of F)

SET-UP

- 9) Report turning inbound to station
- 10) Accelerate to 500 kts
- 11) Report "established \_\_\_ kts, hack"  
    at each airspeed
- 12) Record data

ALTITUDE

KIAS   AOA   IMN   STBY   RESET   RADALT   TAS   PPA

500					4k		
450					4k		
400					4k		
350					4k		
300					4k		
250					4k		

- 13) Accelerate to 350 KIAS
- 14) Turn outbound 3 G's, 350 KIAS
- 15) Report "established in turn, hack"
- 16) Record data

KIAS   AOA   IMN   G's   RADALT

350			3	4K
-----	--	--	---	----

- 17) Climb outbound to 10K

AIRCREW KNEEBOARD CARD #3

Test #3            A-6E

Temp \_\_\_\_\_(C of F)

SET-UP

- 18) Report turning inbound to station
- 19) Establish 250 KIAS, 10K (RESET)
- 20) Report "established \_\_\_\_ kts, hack"  
at each airspeed
- 21) Record data

<u>ALTITUDE</u>						
<u>KIAS</u>	<u>AOA</u>	<u>IMN</u>	<u>STBY</u>	<u>RESET</u>	<u>TAS</u>	<u>PPA</u>
250				10K		
300				10K		
350				10K		
400				10K		
450				10K		
500				10K		

- 22) Slow to 350 KIAS
- 23) Turn outbound 3 G's, 350 KIAS
- 24) Report "established in turn, hack"
- 25) Record data

<u>KIAS</u>	<u>AOA</u>	<u>IMN</u>	<u>G's</u>	<u>RESET</u>
350			3	10K

AIRCREW KNEEBOARD CARD #4

Test #4            A-6E

Temp \_\_\_\_\_(C of F)

SET-UP

- 26) Accelerate to 500 kts, 10K (RESET)
- 27) Report turning inbound to station
- 28) Report "established \_\_\_ kts, hack"  
    at each airspeed
- 29) Record data

<u>KIAS</u>	<u>AOA</u>	<u>ALTITUDE</u>		<u>RESET</u>	<u>TAS</u>	<u>PPA</u>
		<u>IMN</u>	<u>STBY</u>			
500				10K		
450				10K		
400				10K		
350				10K		
300				10K		
250				10K		

- 30) Accelerate to 350 KIAS
- 31) Turn outbound 3 G's, 350 KIAS
- 32) Report "established in turn, hack"
- 33) Record data

<u>KIAS</u>	<u>AOA</u>	<u>IMN</u>	<u>G's</u>	<u>RESET</u>
350			3	10K

AIRCREW KNEEBOARD CARD #5

Test #5            A-6E

Temp \_\_\_\_\_(C of F)

SET-UP

- 34) All runs on inbound leg of racetrack
- 35) Airspeeds listed below, 4K (rad alt)
- 36) Turn outbound 3 G's, try to maintain IMN
- 37) Report "established in turn, hack"
- 38) Record data

CIAS   AOA   IMN   G's   RADALT

250                            3            4K

300                            3            4K

350                            3            4K

400                            3            4K

450                            3            4K

39) RTB

**APPENDIX D**  
**SAIP FLIGHT TEST DATA (27 SEPT 89)**

<b>IRIG TIME</b>	<b>RELATIVE RUN TIME</b>	<b>SPEED (KTAS)</b>	<b>AC ALT (FEET)</b>	<b>SAIP A ALT (FEET)</b>	<b>SAIP B ALT (FEET)</b>	<b>SAIP C ALT (FEET)</b>	<b>SAIP D ALT (FEET)</b>
2:53:40	0.0000	307	10544	9767	9777	9879	9783
2:53:50	0.1667	335	10533	9672	9675	9780	9670
2:54:00	0.3333	364	10513	9636	9610	9731	9632
2:54:10	0.5000	393	10520	9639	9577	9692	9621
2:54:20	0.6667	418	10526	9610	9564	9705	9603
2:54:30	0.8333	443	10538	9551	9436	9603	9544
2:54:40	1.0000	466	10543	9478	9308	9564	9491
2:54:50	1.1667	482	10553	9463	9308	9547	9493
2:55:00	1.3333	498	10559	9377	9308	9452	9404
2:55:10	1.5000	512	10564	9318	9272	9432	9354
2:55:20	1.6667	523	10561	9242	9193	9318	9282
2:55:30	1.8333	533	10556	9203	9178	9314	9258
2:55:40	2.0000	537	10559	9210	92000	9314	9246
2:55:50	2.1667	541	10584	9199	9180	9298	9231
2:56:00	2.3333	532	10597	9226	9206	9318	9243
2:56:10	2.5000	498	10542	9380	9354	9452	9361
2:56:20	2.6667	471	10530	9457	9426	9518	9472
2:56:30	2.8333	446	10526	9524	9462	9603	9528
2:56:40	3.0000	426	10540	9593	9536	9672	9578
2:56:50	3.1667	404	10540	9618	9610	9698	9610
2:57:00	3.3333	382	10527	9656	9665	97411	9665
2:57:10	3.5000	363	10532	9656	9675	9767	9650
2:57:20	3.6667	343	10532	9695	9738	9803	9692
2:57:30	3.8333	327	10520	9706	9747	9793	9711
2:57:40	4.0000	310	10518	9731	9777	9833	9738
2:57:50	4.1667	294	10499	9646	9411	9843	9688
2:58:00	4.3333	284	10492	9679	9749	9843	9685
2:58:10	4.5000	269	10706	9957	9984	10102	9957
2:58:20	4.6667	263	10775	9973	10075	10154	10026
2:58:30	4.8333	268	10504	9742	9842	9888	9744
2:58:40	5.0000	266	10435	9656	9842	9783	9677
2:58:50	5.1667	258	10506	9754	9842	9897	9767
2:59:00	5.3333	252	10564	9852	9869	9974	9850

## LIST OF REFERENCES

1. *Function Specification for the Service Aircraft Instrumentation Package (SAIP)*, Pacific Missile Test Center Specification PMTC-CD-EL-697-76A, 31 March 1989.
2. *Mission Data Summary Tapes*, Numbers 12, 17, 27, and 30, Pacific Missile Test Center, Range Data Processing Center, 27 September 1989.
3. Eastburg, Steve R., *An Engineering Study of Altitude Determination Deficiencies of the Service Aircraft Instrumentation Package (SAIP)*, Aeronautical Engineer's Thesis, Naval Postgraduate School, Monterey, CA, December 1990.
4. NATOPS Flight Manual, A-6E/A-6E Tram/KA-6D Aircraft, NAVAIR 01-85ADF-1.
5. Anderson, John D., *Fundamentals of Aerodynamics*, pp. 280-283, 417-426, McGraw-Hill, Inc., 1984.
6. Shapiro, Ascher M., *The Dynamics and Thermodynamics of Compressible Fluid Flow*, pp. 394-410, The Ronald Press Company, 1953.
7. Lung, Ming-Hung, *Flowfield Measurements in the Vortex Wake of a Missile at High Angle of Attack in Turbulence*, Master's Thesis, Naval Postgraduate School, Monterey, CA, December 1988.
8. Ericsson, L.E., and Reding, J.P., "Asymmetric Vortex Shedding from Bodies of Revolution," *Tactical Missile Aerodynamics*, AIAA, New York, 1986.
9. Telephone conversation between Andy Depuzzo, Grumman Corporation, and the author, 20 August 1991.
10. John, J.E.A., and Haberman, W.L., *Introduction to Fluid Mechanics*, 2nd Edition, p. 25, 1980.
11. Department of Aeronautics, *Laboratory Manual for Low-Speed Wind Tunnel Testing*, Naval Postgraduate School, Monterey, CA, 1989.

## INITIAL DISTRIBUTION LIST

	No. Copies
1. Defense Technical Information Center Cameron Station Alexandria, VA 22304-6145	2
2. Library, Code 52 Naval Postgraduate School Monterey, CA 93943-5002	2
3. Chairman Department of Aeronautics, Code AA Naval Postgraduate School Monterey, CA 93943-5000	1
4. Commander Naval Air System Command (PMA 248) Washington, D.C. 20361	1
5. Mr. Wayne Biesecker Pacific Missile Test Center, Code 3333 Point Mugu, CA 93042-5000	2
6. Mr. James Greer Pacific Missile Test Center, Code 3333 Point Mugu, CA 93042-5000	1
7. Mr. John Loos Pacific Missile Test Center, Code 3333 Point Mugu, CA 93042-5000	1
8. Mr. Guy Cooper Pacific Missile Test Center, Code 9054 Point Mugu, CA 93042-5000	1